Computational Mechanics
https://doi.org/10.1007/s00466-024-02595-w

ORIGINAL PAPER

Artificial neural networks for random fields to predict the buckling load of geometrically imperfect structures

Maximilian Schweizer[1] · **Marc Fina**[1] · **Werner Wagner**[1] · **Steffen Freitag**[1]

Received: 24 October 2024 / Accepted: 26 December 2024

Abstract
The prediction of buckling loads for slender and thin-walled structures under compression loading is important for the structural reliability assessment. The presence of random geometrical imperfections reduces the buckling load and is uncertain. In the framework of a probabilistic buckling analysis, the geometrical imperfections are modeled as correlated random fields and applied on the Finite-Element (FE) model. The buckling analysis is then computed by a Monte Carlo Simulation (MCS). The probabilistic approach in structural engineering demands the assurance of a low probability of failure and thus, high accuracy in the calculation of the probability distribution. The resulting high computational cost of the Monte Carlo Simulation can be reduced with a surrogate model of the FE simulation. The development of an effective surrogate model for random fields is challenging, because of the high dimensional input. In this work, an artificial neural network (ANN) surrogate model is presented, to predict the buckling load of structures considering random fields of geometrical imperfections as input. The training procedure is based on random field and the corresponding buckling load samples obtained from FE simulations. The trained ANN surrogate model is finally applied within a MCS-loop, yielding the probability distribution of the buckling load. Three numerical examples (column, plate and cylindrical shell segment) demonstrate that the ANN is able to learn the input-output relationship for structures with different buckling behaviors. The results are compared with a reference FE solution and the computation time shows, that the presented method is an efficient way to speedup the MCS. It is shown that the ANNs learning ability depends on the correlation length of the random field realizations.

Keywords Artificial neural network · Surrogate model · Random field · Stochastic buckling analysis · Geometrical imperfection · Karhunen-Loeve-Expansion

1 Introduction

Buckling failure is very critical in structural engineering. It is well known from experiments, that buckling loads can have large deviations from the theoretical values [1]. One of the main reasons for this phenomenon are geometrical imperfections of the structures surface [2, 3]. Especially for thin-walled shell structures, the experimental values are significantly lower than the theoretical values. In order to account for this buckling load reduction, the NASA SP-8007 guideline from 1968 [4] developed the "knock-down" curves as a lower limit of the buckling load, depending on the shell's radius to thickness ratio. This semi-empirical approach leads to a conservative structural design. Deterministic approaches are in general not reliable for the buckling load prediction of structures that are sensitive to imperfections, e.g., thin-walled shells [5]. Since imperfections are of random nature, a more reliable method to predict the buckling load, is the probabilistic approach [5–8]. In [9], the measured imperfections are transformed to a Fourier series considering random variables as coefficients. Another method to describe random imperfections as random fields is the Karhunen-Loeve-Expansion (KLE) method [10–12], which is used in this paper. Realizations of random field imperfections are used as inputs of the FE model and the numerical buckling analysis yields the

✉ Maximilian Schweizer
maximilian.schweizer@kit.edu

Marc Fina
marc.fina@kit.edu

Werner Wagner
werner.wagner@kit.edu

Steffen Freitag
steffen.freitag@kit.edu

[1] Institute for Structural Analysis, Karlsruhe Institute of Technology, Kaiserstrasse, 12, 76131 Karlsruhe, Germany

Published online: 11 February 2025

buckling load of the imperfect structure. This procedure is repeated in a Monte Carlo Simulation (MCS) resulting in the probability distribution of the buckling load. Imperfection modeling with random fields in buckling analysis, especially for shell structures, has been widely investigated in [10, 13]. Also in other engineering disciplines, the application of random field modeling has been very useful, see, e.g.: the soil properties in geotechnical engineering [14, 15] and the modeling of spatial variability in concrete [16].

The MCS is known for its high computation time depending on the complexity of the deterministic solution (FE model) and the required amount of samples, which depends on the stochastic quantity of interest. The mean value and variance, e.g., have a faster convergence, compared to low probabilities. In the framework of a probabilistic safety assessment in civil engineering, the stochastic quantity of interest is the probability of failure, which must be guaranteed to be lower than a given threshold value. According to the guideline DIN EN 1990 [17], a reliability index β is given, which can directly be translated in an accepted probability of failure in the range of $P_f = 10^{-5}$ to 10^{-3}, dependent on the consequence class. The calculation of such a low probability of failure requires a very precise probability distribution, i.e., a very high number of Monte Carlo Simulations leading to high computation time, especially for large and complex structures. The computation time is strongly increased by adding more uncertain variables to the model, as for example fuzzy or interval variables considering epistemic uncertainty. An example are random field correlation parameters, leading to polymorphic random fields in numerical buckling analysis, which has been investigated in [18–21]. Even more variables are required in the framework of a structural design optimization, see, e.g., [22–24] for a reinforced concrete bridge, [25] for a wooden structure and [26] for a shell structure. The combination of different types of variables (uncertain variables and design variables) increases the computation time drastically. Therefore, efficient surrogate models are of crucial importance to reduce the computation time. Surrogate models replace the FE simulation model by approximating the relationship between input and output variables. Some examples for the application of surrogate models in structural engineering problems are: multilevel surrogate modeling for optimization with polymorphic uncertain parameters [22], bounding failure probabilities in imprecise stochastic FE models [27, 28], structural response prediction of buildings [29, 30], uncertain pedestrian load modeling in footbridge design [31] and control-variates method in shell buckling [21, 32].

In recent publications, artificial neural networks (ANNs) are used for the prediction of buckling loads with material and structural parameters as input variables, see, e.g., [33–35]. ANNs with random field inputs are already used, e.g. in geotechnical engineering [36, 37]. In the particular case of shell buckling problems, the application of ANNs on random fields is very rare. One recent example is [38], where a convolutional neural network is applied on a random field to predict the buckling load of a cylinder with measured imperfections in real-time. However, the training performance with respect to the shape of the imperfections is not investigated.

This paper presents a surrogate model based on feed-forward ANNs to predict the buckling load of structures with random imperfections. The main goal is to speedup the MCS to obtain the probability distribution of the buckling load, while consuming less computation time compared to the FE solution. The novelty of the method lies in the choice of the input variables, which are the uncorrelated Gaussian random numbers of the KLE series instead of the random imperfection values. The advantage of the chosen approach, is the possibility of input reduction by truncating the KLE series. This has significant influence on the training performance and thus, the quality of the predicted probability distribution. Another advantage is the possibility of analyzing the input variables sensitivity on the buckling load. The highlights of this paper are summarized as follows:

- Buckling load prediction of geometrically imperfect structures with ANN
- Reduced random field input for ANN training
- Investigation of the correlation lengths influence on the ANN training performance
- Time saving of Monte Carlo Simulations with trained ANNs

The buckling analysis with random imperfections is explained in Sect. 2. Subsequently, the ANN training strategy is elaborated in Sect. 3. In Sect. 4, the numerical examples are shown on three different structures (column, plate and shell) with different buckling behavior to demonstrate the method's utility. The results are compared with an FE reference solution. The influence of the random field's correlation and the number of samples in the training set on the model quality is investigated. Finally, the error of the ANN is measured and the computation time of the ANN and the FE solution is compared. The conclusions and future research topics are discussed in Sect. 5.

2 Buckling analysis with random imperfections

This section contains two subsections, explaining the basic principles for the modeling of geometrical imperfections as random fields in buckling analysis. At first, the random field theory and the KLE method is briefly described in Sect. 2.1. Especially the truncated KLE is important for the input dimension reduction. Afterwards, the basics of nonlin-

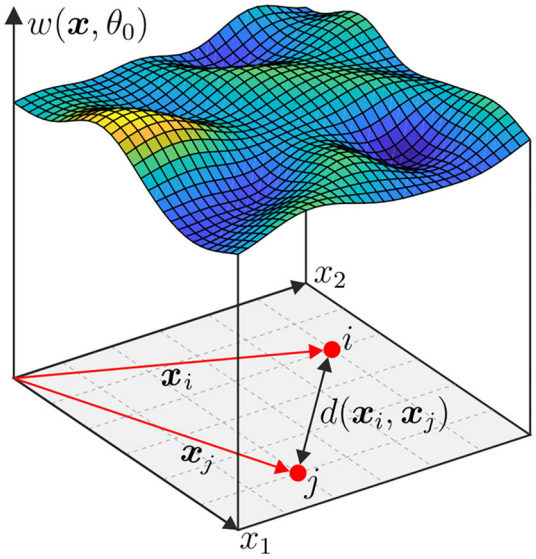

Fig. 1 Realization of a two dimensional random field $w(\boldsymbol{x}, \theta_0)$ and two generic points i and j with respective vectors $\boldsymbol{x}_i$ and $\boldsymbol{x}_j$ and their distance $d(\boldsymbol{x}_i, \boldsymbol{x}_j)$

ear buckling analysis are introduced within the context of stochastic buckling analysis in Sect. 2.2.

2.1 Random field modeling for geometrical imperfections

Geometrical imperfections are deviations from the nominal surface. They are modeled as correlated random fields and applied on the FE model of the structure as stress-free displacements. The basics of the random field theory and the KLE method are briefly summarized based on [39, 40].

Given the surface of a structure as domain Ω and the location vector $\boldsymbol{x}$, the surface deviations $w(\boldsymbol{x})$ are random and, therefore, modeled as correlated random field.

A random field $w(\boldsymbol{x}, \theta)$ is a scalar field that assigns a random value at each point $\boldsymbol{x} \in \Omega$ and for each event $\theta \in \Theta$, where Θ is the set of possible events. Thus, a random field is a set of random variables

$$\{w(\boldsymbol{x}, \theta) \mid \boldsymbol{x} \in \Omega, \theta \in \Theta\} \ . \tag{1}$$

A Gaussian random field is completely defined by its mean $\mu(\boldsymbol{x})$, variance $\sigma^2(\boldsymbol{x})$ and autocorrelation coefficient $\rho(\boldsymbol{x}_i, \boldsymbol{x}_j)$. Further, if the mean and variance are constant within the domain and if ρ only depends on the difference $\boldsymbol{x}_i - \boldsymbol{x}_j$, the field is called "homogeneous". In Fig. 1, a realization of a two dimensional random field is presented.

For the numerical implementation into an FE model, the random field is discretized according to the FE nodes. The random field is modelled with the Karhunen-Loeve-Expansion (KLE) method, introduced in [41], which is a series expansion method based on the spectral decomposition of its covariance function

$$C(\boldsymbol{x}_i, \boldsymbol{x}_j) = \sigma^2 \rho(\boldsymbol{x}_i, \boldsymbol{x}_j) \ . \tag{2}$$

Evaluating C for each pair of points $(\boldsymbol{x}_i, \boldsymbol{x}_j) \in \Omega$, the covariance matrix

$$\boldsymbol{C}_{N\times N} = \begin{bmatrix} C(\boldsymbol{x}_1, \boldsymbol{x}_1) & \dots & C(\boldsymbol{x}_1, \boldsymbol{x}_N) \\ \vdots & \ddots & \vdots \\ C(\boldsymbol{x}_N, \boldsymbol{x}_1) & \dots & C(\boldsymbol{x}_N, \boldsymbol{x}_N) \end{bmatrix} \ , \tag{3}$$

is obtained, where N is the total number of nodes in the FE mesh. The deterministic functions used to expand any realization of the field $w(\boldsymbol{x}, \theta_0)$, are determined by solving the eigenvalue problem of the covariance matrix

$$\boldsymbol{C}\boldsymbol{\varphi}_i = \lambda_i \boldsymbol{\varphi}_i \ , \tag{4}$$

which is symmetric and positive definite. Thus, the discrete random field is written as

$$\widehat{w}(\boldsymbol{x}, \theta) = \mu + \sigma \sum_{i=1}^{N} \xi_i(\theta) \sqrt{\lambda_i} \varphi_i(\boldsymbol{x}) \ , \tag{5}$$

where $\xi_i(\theta)$ is a standard normal distributed random variable $\xi_i(\theta) \sim \mathcal{N}(0, 1)$. As the random field is used to describe the deviations from the reference surface, the mean value is set to zero $\mu = 0$. The standard deviation is set to $\sigma = 1$ in this paper.

For the autocorrelation function $\rho(\boldsymbol{x}_i, \boldsymbol{x}_j)$, a quadratic exponential function is used

$$\rho(\boldsymbol{x}_i, \boldsymbol{x}_j) = \exp\left(-\frac{d^2(\boldsymbol{x}_i, \boldsymbol{x}_j)}{\ell_c^2}\right) \ , \tag{6}$$

with the correlation length ℓ_c and the distance between two FE nodes

$$d(\boldsymbol{x}_i, \boldsymbol{x}_j) = |\boldsymbol{x}_i - \boldsymbol{x}_j| \ . \tag{7}$$

The quadratic exponential autocorrelation function has the advantage, that it realizes smooth random fields and requires less terms in the KLE series, compared to non-differentiable autocorrelation functions and is therefore, commonly used in random field modeling. In [18, 42], it is shown, that correlation functions determined from measurements yield realistic geometrical imperfections, due to the infinite differentiability. The developed surrogate modeling approach is demonstrated based on the quadratic exponential function. However, the approach can also be applied to random fields with other correlation functions. The use of Gaussian autocorrelation functions is discussed in [43, 44].

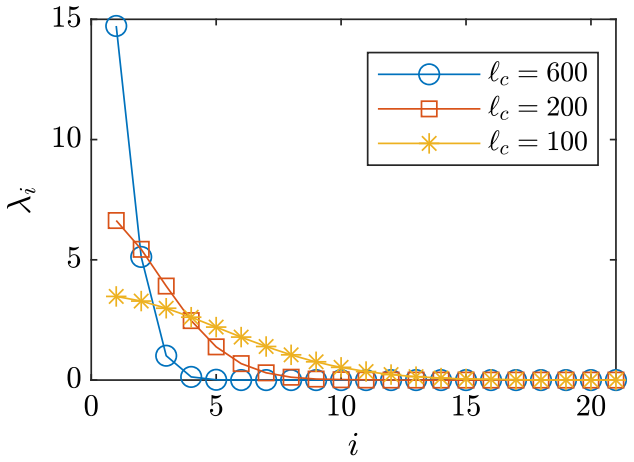

Fig. 2 Sorted eigenvalues λ_i of the covariance matrix via index of eigenvalues i for one dimensional random fields of length $L = 1000$ with different correlation lengths ℓ_c

An important characteristic of the eigenvalues λ_i of the covariance matrix according to Eq. (3) is, that they can be sorted in a descending order converging to zero. Truncating the series in Eq. (5) after the n-th term yields the approximated random field

$$\widehat{w}(\boldsymbol{x}, \theta) = \mu + \sum_{i=1}^{n} \xi_i(\theta) \sqrt{\lambda_i} \varphi_i(\boldsymbol{x}). \tag{8}$$

The decrease of sorted eigenvalues λ_i of the covariance matrix depends on the correlation length ℓ_c. This is visualized for a one dimensional random field of length $L = 1000$ with different correlation lengths ℓ_c in Fig. 2. The higher the correlation length ℓ_c, the higher is the decrease rate of the eigenvalues λ_i of the covariance matrix.

The required number n of considered eigenvalues in the KLE can be determined with the quality index, given in [45]

$$Q = \frac{1}{\mathrm{tr}(\boldsymbol{C})} \sum_{k=1}^{n} \lambda_k \ . \tag{9}$$

A quality index of $Q = 1$ means that all eigenvalues are considered. A quality index lower than one $Q < 1$ reduces the required number of eigenvalues λ_i and thus the input variables. However, it also decreases the approximation quality of the correlated random field. In most cases a quality index of $Q = 0.99$ is used [13].

2.2 Numerical Buckling analysis of imperfect structures

The modeling of random imperfections leads to the stochastic buckling analysis, where the probability distribution of the buckling load is calculated with Monte Carlo Simulations of random field realizations. The buckling analysis introduced in this section is based on [32, 46].

When a structure is subjected to an incrementally increasing compression load, it will reach a critical point (stability point) and suddenly deform with a huge load bearing capacity loss. This phenomenon is called buckling and the load level at this point is called critical buckling load or buckling load. At the critical buckling load level, the structure is in an indifferent equilibrium state and the tangent stiffness matrix $\boldsymbol{K}_T$ is singular.

In order to find a stability point, it can be distinguished between linear and nonlinear buckling analysis. For structures with linear pre-buckling behavior the linear buckling analysis is sufficient, which is based on the decomposition of the tangent stiffness matrix

$$\boldsymbol{K}_T = \boldsymbol{K}_{\mathrm{lin}} + \boldsymbol{K}_{\mathrm{nlin}} \ , \tag{10}$$

where the stiffness matrix is divided into linear $\boldsymbol{K}_{\mathrm{lin}}$ and nonlinear $\boldsymbol{K}_{\mathrm{nlin}}$ parts. With an external load $\boldsymbol{P}_0$ the displacements $\boldsymbol{u}_0$ can be calculated with the linear solution

$$\boldsymbol{K}_T(\boldsymbol{0})\boldsymbol{u}_0 = \boldsymbol{P}_0 \quad \Longleftrightarrow \quad \boldsymbol{u}_0 = \boldsymbol{K}_T(\boldsymbol{0})^{-1}\boldsymbol{P}_0 \ , \tag{11}$$

with $\boldsymbol{K}_T(\boldsymbol{0}) = \boldsymbol{K}_{\mathrm{lin}}$. The linear buckling analysis consists in the solution of the eigenvalue problem

$$[\boldsymbol{K}_{\mathrm{lin}} + \Lambda \boldsymbol{K}_{\mathrm{nlin}}]\boldsymbol{\varphi} = \boldsymbol{0} \ , \tag{12}$$

which leads to a critical buckling load factor Λ_{cr} and the initial postbuckling mode $\boldsymbol{\varphi}$. The critical buckling load with the corresponding critical displacement can be calculated by

$$\boldsymbol{P}_{\mathrm{cr}} = \Lambda_{\mathrm{cr}} \boldsymbol{P}_0 \ , \quad \boldsymbol{u}_{\mathrm{cr}} = \Lambda_{\mathrm{cr}} \boldsymbol{u}_0 \ . \tag{13}$$

For thin-walled structures with nonlinear prebuckling behavior, the linear buckling analysis can strongly differ from the correct buckling load. In that case, a nonlinear buckling analysis is required, where a complete geometrically nonlinear path following algorithm is used. It consists in the incremental calculation of the load-displacement curve, while observing the diagonal signs of the tangent stiffness matrix $\boldsymbol{K}_T$, with the following statements

$$\begin{aligned} &\forall D_{ii} \ , \ D_{ii} > 0 \rightarrow \text{stable} \\ &\exists D_{ii} \ , \ D_{ii} = 0 \rightarrow \text{indifferent} \\ &\exists D_{ii} \ , \ D_{ii} < 0 \rightarrow \text{unstable.} \end{aligned} \tag{14}$$

The load-displacement curves for three structure types (column, plate and cylindrical shell segment) investigated in this paper are shown in Fig. 3. The load starts at zero and is increased stepwise. The column and the plate show a linear pre-buckling behavior. The structure without imperfections

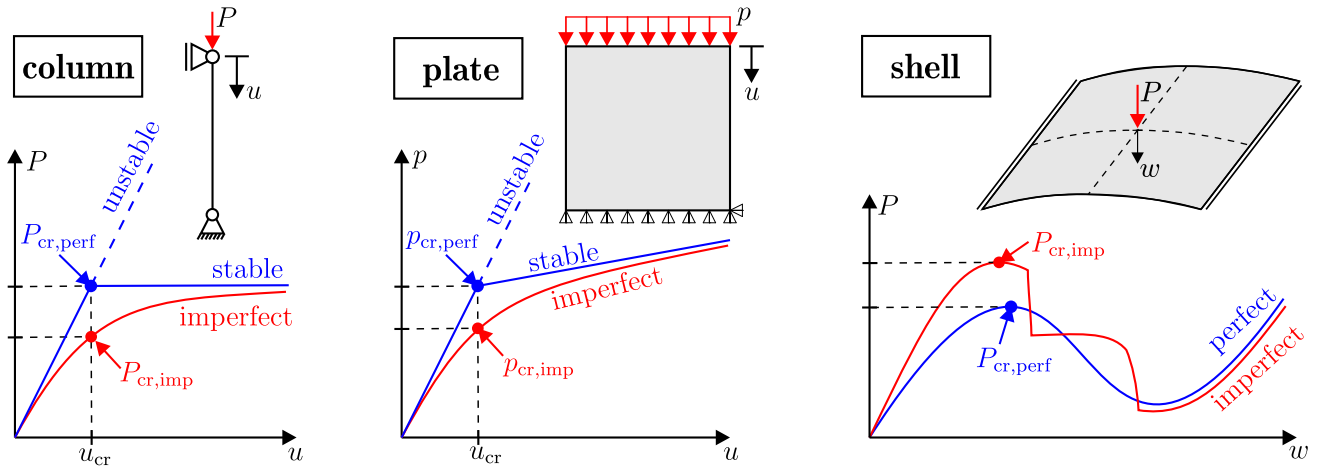

Fig. 3 Load-displacement curves for a column, a plate and a cylindrical shell segment with and without imperfections

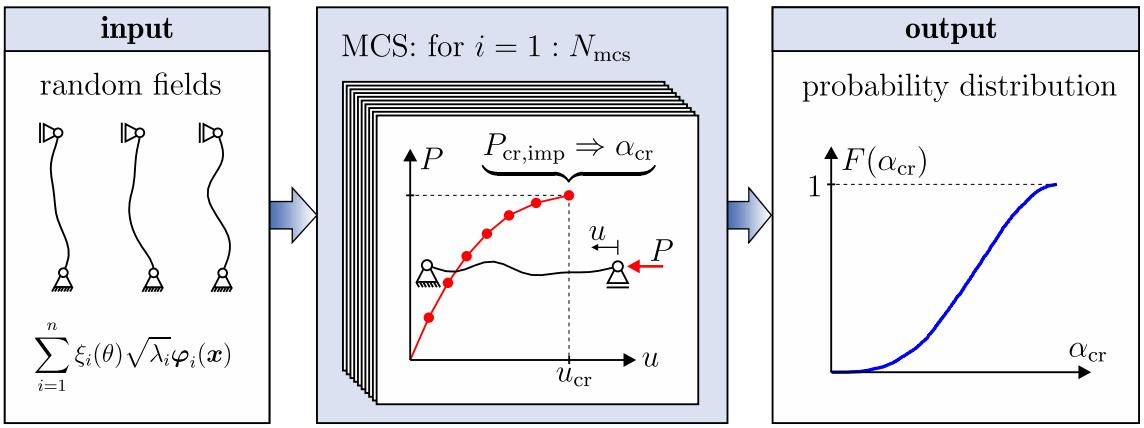

Fig. 4 Stochastic buckling analysis with random imperfections

is referred to as "perfect" structure. The perfect structure follows the primary (unstable) path, shown with a linear dashed line. A small imperfection at the stability point deflects the structure to follow the secondary (stable) path. The imperfection is the first eigenmode, applied as geometrical deviation on the structure at the stability point, where the equilibrium splits into two different paths. The stability point is therefore called "bifurcation point". The load and displacement values at the stability point are $P_{\text{cr, perf}}$ and u_{cr}. The structure with geometrical imperfections is referred to as "imperfect" structure. The imperfect structure, modeled with a correlated random field, follows a non-linear load-displacement curve and has no stability point. However, large deformations with a noticeable load bearing capacity loss can be observed. Therefore, the evaluation point for the critical buckling load of the imperfect structure $P_{\text{cr, imp}}$ is the load level at u_{cr}. The cylindrical shell segment on the other hand shows a very particular load-displacement curve with a non-linear pre-buckling behavior. The stability point is a limit point, where the load-displacement curve reaches a local maximum. The limit point does still exist for the imperfect structure.

An important value for the structural stability assessment is the critical buckling load factor α_{cr}, which is the ratio between the buckling loads with and without imperfections

$$\alpha_{\text{cr}} = \frac{P_{\text{cr, imp}}}{P_{\text{cr, perf}}} \quad . \tag{15}$$

The load-displacement curves are computed with an iterative path-following algorithm. A well known algorithm is the arc-length-method [47, 48]. The displacement controlled arc-length method is used for the nonlinear buckling analysis in the Finite Element Analysis Program (FEAP) [49].

Because the imperfections are random, multiple random field realizations are applied on the structure in a Monte Carlo Simulation. For each random field sample, the numerical nonlinear buckling analysis is carried out on the imperfect structure until a stability point is found, yielding the buckling load samples. The stochastic buckling analysis is represented in Fig. 4. The inputs are the random field samples computed

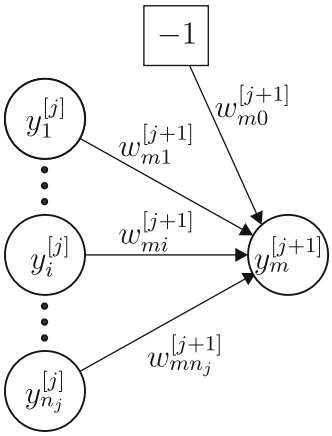

Fig. 5 Signal processing of one neuron with weighted connections and bias neuron

with the KLE and the output is the probability distribution of the critical buckling load factor α_{cr}. The probabilistic approach in civil engineering demands the guarantee of a very low probability of failure $P_f = 10^{-5} - 10^{-3}$ [17]. Therefore, the MCS requires a very high number of samples N_{mcs}, which is highly time consuming. The computation time increases even more with the complexity of the structure. Therefore, a time saving surrogate model is of crucial importance to enhance the overall modeling capacity. In the following section, a new artificial neural network (ANN) surrogate model is developed to speedup the MCS in the context of structural stability analysis.

3 ANN training with random field input

In this section, the ANN surrogate modeling strategy is introduced. The aim is to predict the buckling load of a structure with a random geometrical imperfection. The trained ANN is used as surrogate model in the stochastic buckling analysis to predict the probability distribution of the buckling load.

In general, a surrogate model $\widehat{\mathcal{M}}(\boldsymbol{x})$ is an approximation of a functional operator $\mathcal{M}(\boldsymbol{x})$. Surrogate models are used when the analytical solution is not available and the numerical computation is too expensive, see, e.g., [22]. Artificial neural networks are often used in machine learning applications and have shown over the years to be effective surrogate models to solve engineering problems, especially when dealing with a high dimensional input [50, 51].

ANNs consist of connected layers of nodes called neurons. The most common type of an ANN is the feed-forward neural network where the information flows in one direction from the input to the output layer.

The signal processing of one arbitrary neuron $y_m^{[j+1]}$ is depicted in Fig. 5, where the neurons are represented as circles and the weights as arrows. In each layer j there is one bias neuron with value -1 connected to each neuron $y_m^{[j]}$ with the weight $w_{m0}^{[j]}$. The output of a neuron is the weighted sum of all inputs passed through an activation function according to the following equation

$$y_m^{[j+1]} = f\left(\sum_{i=0}^{n_j} w_{mi} \cdot y_i^{[j]}\right) \ , \tag{16}$$

where $f(x)$ is the activation function and w_{mi} are the weights between neuron m and i. Here, the activation function is the hyperbolic tangent function $\tanh(x)$. The output of one neuron is processed forward as weighted input in the connected neurons of the next layer. In this way the information propagates forward layer by layer until the output layer is reached.

The unknown weights of the ANN are adjusted during the ANN training. The set of all available samples N_{train} (training set) is split randomly in training (70%), validation (15%) and testing (15%) samples. For the computational implementation, MATLAB [52] has been used. The complete propagation of all samples from the input to the output layer, is called epoch. After one epoch, the weights are adjusted to minimize the loss function error of the output through a backpropagation algorithm, which is here selected as the Levenberg-Marquardt backpropagation [53, 54]. The mean square error (MSE)

$$\text{MSE} = \frac{1}{N_{\text{tr}}} \sum_{i=1}^{N_{\text{tr}}} (\alpha_{\text{cr},i} - \widehat{\alpha}_{\text{cr},i})^2 \tag{17}$$

of the training samples N_{tr} is selected as loss function, where α_{cr} is the reference (FE) solution and $\widehat{\alpha}_{\text{cr}}$ is the predicted solution, i.e. the ANN solution. The MSE of the validation samples is used to stop the training process (minimal validation error) and the generalization performance of the ANN is evaluated based on the MSE of the testing samples.

For the choice of the ANN input variables in this particular application, there are two options: the random field itself $\widehat{w}(\boldsymbol{x}, \theta)$, i.e. the random geometrical deviations of the FE nodes or the random numbers $\xi_i(\theta)$ in the KLE (8), which are each one affiliated to an eigenvalue λ_i and eigenvector $\varphi_i(\boldsymbol{x})$. The two options are represented in Eqs. (18) and (19)

$$\widehat{\mathcal{M}}(\widehat{w}(\boldsymbol{x}, \theta)) \mapsto \alpha_{\text{cr}} \ , \tag{18}$$

$$\widehat{\mathcal{M}}(\boldsymbol{\xi}(\theta)) \mapsto \alpha_{\text{cr}} \ , \tag{19}$$

where $\boldsymbol{\xi}(\theta)$ is the vector of random numbers: $\boldsymbol{\xi} = [\xi_1(\theta)\ \xi_2(\theta)\ \ldots\ \xi_n(\theta)]$. In Eq. (18), the number of inputs is constant and equal to the number of FE nodes. In Eq. (19), it is possible to reduce the number of inputs by truncating the series with a quality index $Q < 1$. The number of input neurons has a significant influence on the ANN training process, where less neurons leads to less training data and training time needed.

Therefore, the second option with the random numbers $\xi_i(\theta)$ as input, according to Eq. (19), is proposed as novel approach.

The particular characteristic of this ANN is, that the number of input neurons is variable, depending on the random field's correlation length ℓ_c and quality index Q. There is only one output neuron, which is the critical buckling load factor α_{cr}. The ANN surrogate model strategy is visualized in Fig. 6. Firstly, for a given correlation length ℓ_c the eigenvalue problem of the covariance matrix $\boldsymbol{C}$ is solved. The eigenvalues λ_i and eigenvectors $\boldsymbol{\varphi}_i$ are required for the KLE. Subsequently, the training, validation and testing samples, which consist of input $\boldsymbol{\xi}$ and output α_{cr} pairs, are generated with the FE solutions to compute $P_{\text{cr,perf}}$ and $P_{\text{cr,imp}}$.

Each sample $\boldsymbol{\xi}$ is inserted in the KLE and yields one realization of the random field, which is applied on the FE model as geometrical imperfection. Then, the nonlinear FE buckling analysis is computed on the imperfect structure, the load-displacement curve is calculated and $P_{\text{cr,imp}}$ is determined.

The buckling load factor α_{cr} is saved and the procedure is repeated N_{train} times with N_{train} different samples of $\boldsymbol{\xi}$. After successful training, the ANN surrogate model is used to generate the desired number N_{mcs} of Monte Carlo Simulations, and thus the probability distribution of α_{cr} is obtained.

The required amount of samples in the training set N_{train} depends on the total number of training parameters, i.e. the weights, and can be calculated as follows

$$N_{\text{para}} = \sum_{i=1}^{N-1} (n_i + 1) \cdot n_{i+1} \ , \tag{20}$$

where $N = 5$ is the total number of layers including input and output layer and n_i is the number of neurons in the i^{th} layer. For a given quality index Q, the number of input variables n and thus the number of input neurons depends on the random field's correlation length ℓ_c. Therefore, the influence of the correlation length ℓ_c on the ANN training quality is investigated in the next section.

4 Numerical examples

In this section, the presented method is investigated for three different structure types: a column, a plate and a cylindrical shell segment. The range of the correlation lengths is chosen with respect to the structural dimensions in the interval $\ell_c \in [0.2L,\ 0.5L]$, based on investigations from a preliminary work [18]. The structures show different buckling behavior, which has an influence on the ANN training performance. The sensitivity of the input variables $\xi_i(\theta)$ is investigated comparing FE and ANN solutions. The ANN training is carried out for different correlation lengths and different amount of samples in the training set. For each

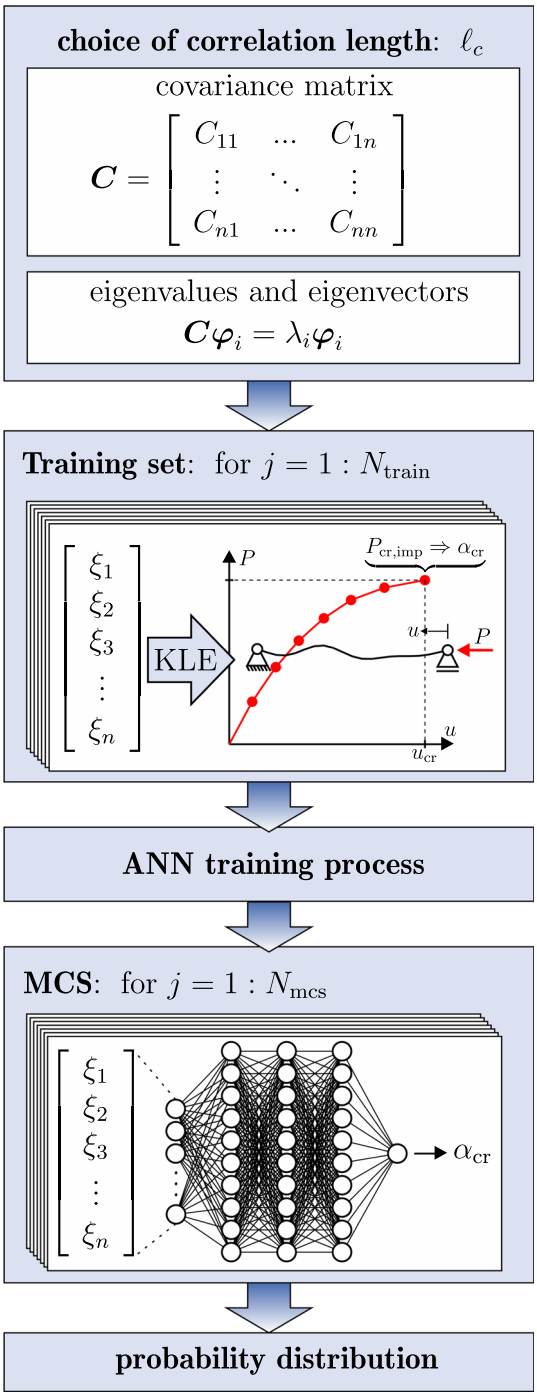

Fig. 6 Representation of the ANN surrogate modeling strategy

training setting, the ANN training process is repeated 5 times with new realizations of imperfections to observe the training robustness. The presented surrogate model is a simple feed-forward ANN with three fully connected hidden layers with 10 neurons in each one. Because the number of input variables differs for each correlation length ℓ_c, the ANN architecture is calibrated with the maximal number of input variables, i.e. the lowest investigated correlation length ℓ_c

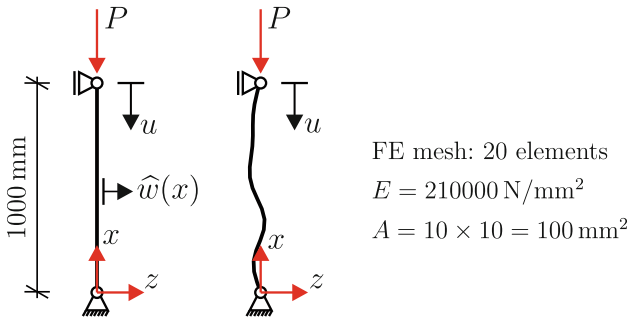

Fig. 7 Euler column case 2 without and with imperfection for a random field realization with $\ell_c = 200\,\text{mm}$

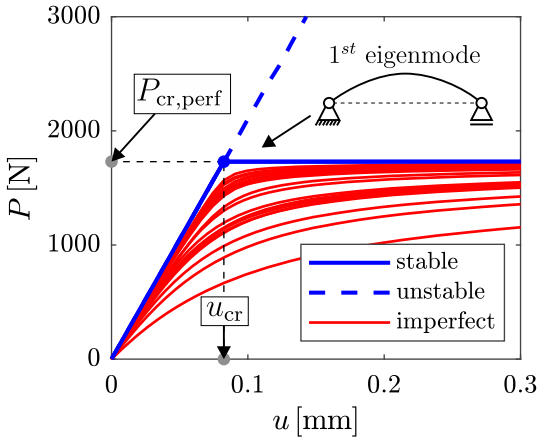

Fig. 8 Load displacement curves of the column without and with imperfections for $\ell_c = 200\,\text{mm}$

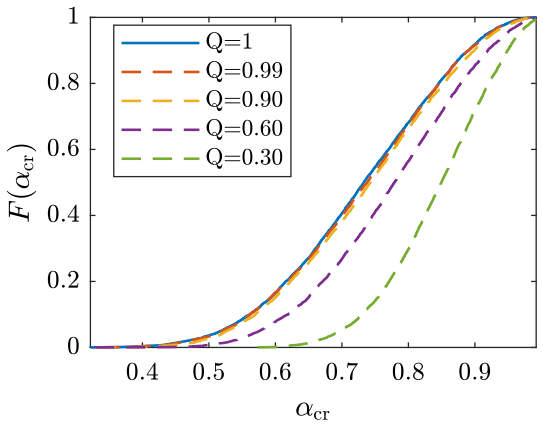

Fig. 9 CDFs for the critical buckling load factor α_{cr} with 5000 samples, $\ell_c = 200\,\text{mm}$ and different quality indices Q

for each example. It has been found, that three hidden layers with 10 neurons in each one are sufficient for all presented examples.

The results are compared with an FE reference solution of 5000 MCS samples. Of course, the required number of MCS samples can be higher, dependent on the stochastic quantity of interest. The ANN performance is measured with the root mean squared error (RMSE) summarized in a box-plot diagram and the ANN computation time is compared with the computation time for the FE-MCS. In order to demonstrate the ANNs benefit, a low probability of failure is calculated for the last example, thus requiring a very high number of MCS.

4.1 Euler column

The first example, serving as a proof of concept, is a two dimensional simply supported Bernoulli beam. The structure without and with imperfection with $\ell_c = 200\,\text{mm}$ is shown in Fig. 7. The buckling load of the column without imperfections is given by Euler's formula [55]

$$P_{\text{cr,perf}} = \frac{\pi^2 E I}{L^2} = 1727.18\,\text{N} \ . \tag{21}$$

The same value is calculated with the numerical buckling analysis. The load-displacement curve in Fig. 8 shows a linear pre-buckling behavior for the structure without imperfections with a critical displacement of $u_{\text{cr}} = 0.0824\,\text{mm}$. The type of stability point is a bifurcation point. In order to follow the post-buckling path, the first eigenmode with an amplitude of 1 mm is applied on the structure at the bifurcation point. In the post-buckling path, the column is subject to large displacements with negligible load increase, which almost corresponds to a horizontal line. The load-displacement curve for the imperfect structure is computed with a one dimensional random field with a correlation length of $\ell_c = 200\,\text{mm}$ and a quality index of $Q = 0.99$. This computation is repeated multiple times to show the randomness of the load-displacement curves. With geometrical imperfections, the bifurcation point disappears. Therefore, the critical buckling load for the imperfect structure $P_{\text{cr,imp}}$ is defined as the load at u_{cr}. The critical buckling load of the structure with geometrical imperfections is lower than the critical buckling load of the structure without imperfections. Thus, the critical buckling load factor α_{cr} is lower than 1.

The load-displacement curves are computed in a Monte Carlo Simulation, yielding $N_{\text{mcs}} = 5000$ samples of the critical buckling load factor α_{cr}. The same MCS is repeated for different quality indices Q and the cumulative distribution functions (CDFs) are shown in Fig. 9. The corresponding number of input variables N_{input} is calculated according to Eq. 9 and given in Table 1. The aim is to minimize the input variables, while still ensuring an accurate approximation of the complete quality of the KLE series. The CDFs in Fig. 9 with $Q = 0.99$ and $Q = 0.90$ show a good approximation of $Q = 1$. The quality index of $Q = 0.99$ is chosen for all further examples because it offers the most significant input reduction factor.

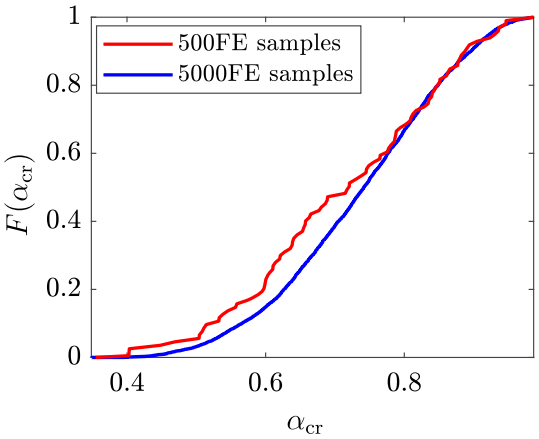

Fig. 10 CDFs with 500 and 5000 FE samples for the column with $\ell_c = 200\,\text{mm}$

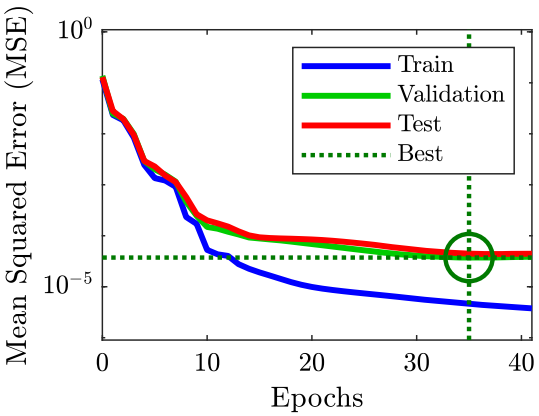

Fig. 11 Loss function evolution via training epochs of one ANN training process for the column with $\ell_c = 200\,\text{mm}$ and a training set with 500 samples

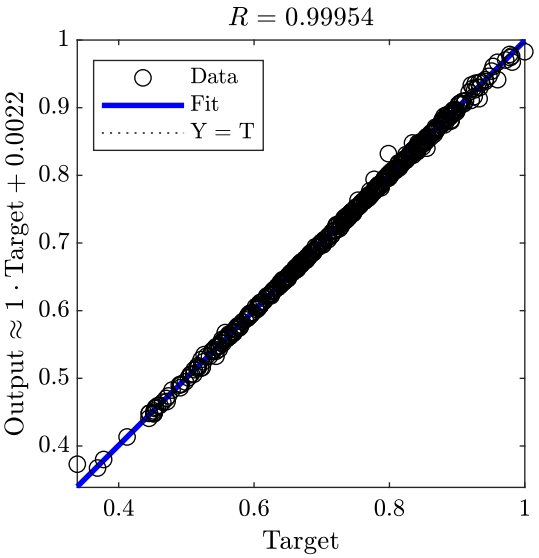

Fig. 12 Regression plot for training, testing and validation samples for one ANN training process for the column with $\ell_c = 200\,\text{mm}$ and a training set with 500 samples

Table 1 Quality index Q and number of input variables N_{input} for the column with $\ell_c = 200\,\text{mm}$

Q	1	0.99	0.9	0.6	0.3
N_{input}	21	7	5	3	1

Sample 1	Sample 2	Sample 3
ξ_1: -1.651, 1.449, -1.530, -0.064, -0.736, 0.803, -0.119	ξ_2: -0.611, 0.706, -2.189, -1.266, -1.335, -0.252, -1.085	ξ_3: 0.694, 1.026, -1.478, 0.504, 1.430, -0.578, 0.795
$\alpha_{\text{cr,FE}} = 0.746$ $\alpha_{\text{cr,ANN}} = 0.745$	$\alpha_{\text{cr,FE}} = 0.506$ $\alpha_{\text{cr,ANN}} = 0.506$	$\alpha_{\text{cr,FE}} = 0.792$ $\alpha_{\text{cr,ANN}} = 0.793$

Fig. 13 Three random samples of the imperfect column with $\ell_c = 200\,\text{mm}$ and the corresponding FE and ANN solutions for the critical buckling load factor based on a training set with 500 samples

By truncating the KLE with a quality index of $Q = 0.99$, the random field has $N_{\text{input}} = 7$ input variables. Thus, the number of training parameters are calculated to $N_{\text{para}} = 311$ according to Eq. (20). This number is used as an estimation of the lower limit for the required number of training samples.

The first ANN training procedure is carried out with a training set with $N_{\text{train}} = 500$ samples. The CDFs with 500 and 5000 FE samples are depicted in Fig. 10, to show the scattering of 500 MCS samples compared to the reference solution. Instead of computing 5000 MCS samples, the 500 available samples are utilized to train the ANN function, enabling it to generate more samples with reduced computational effort.

The training loss function, depicted in Fig. 11, shows the MSE of the training, validation and testing sets in each epoch. The best validation performance is $3.74 \cdot 10^{-5}$ at epoch 35. The regression plot for training, validation and testing samples, depicted in Fig. 12, shows each output and target value as one point on the graph. The points lie on the angle bisector, which indicates a successful training process. Three exemplary samples of imperfections $\boldsymbol{\xi}$ and output α_{cr} are depicted in Fig. 13 with FE and ANN solutions. The predicted values are accurate up to the second decimal place.

With the ANN function, 5000 MCS are carried out to obtain the probability distribution of the buckling load. The ANN training is repeated five times with five independent sets of samples in order to test the training robustness. In Fig. 14, the CDFs of 5000 MCS samples of the ANN solution are compared with the FE solution. The five CDFs in Fig. 14 are almost indistinguishable. A zoom in the range of $\alpha_{\text{cr}} =$

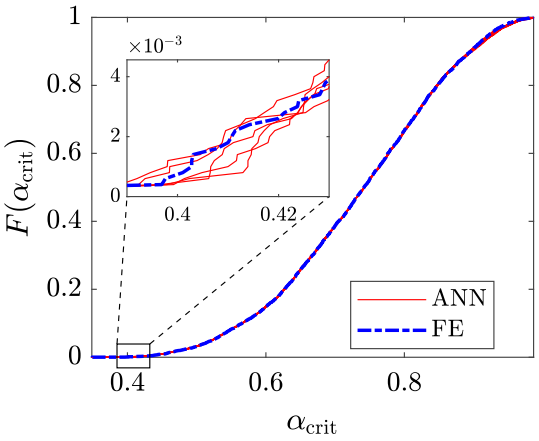

Fig. 14 CDFs of 5000 MCS samples with $\ell_c = 200$ mm. Comparison between the FE solution and five ANN solutions based on five training repetitions with a training set with 500 samples

Table 2 Mean value μ and coefficient of variation CV [%] of the critical buckling load factor and percentage error ε [%] of the five ANN-CDFs compared with the FE-CDF with 5000 Monte Carlo samples of the trained ANN with $\ell_c = 200$ mm and a training set with 500 samples

	μ	$\varepsilon(\mu)$ [%]	CV [%]	$\varepsilon(CV)$ [%]
FE	0.7329	–	16.80	–
ANN_1	0.7349	0.27	16.57	1.39
ANN_2	0.7354	0.33	16.66	0.85
ANN_3	0.7353	0.32	16.69	0.64
ANN_4	0.7350	0.28	16.75	0.29
ANN_5	0.7353	0.32	16.62	1.04

[0.39, 0.43] shows the scattering of the five CDFs. The mean value μ, coefficient of variation CV and respective errors ε of the five ANN solutions are given in Table 2. It is shown, that the surrogate model is robust and able to predict the buckling load samples and to yield the correct probability distribution with an error of approximately 1% for the chosen training setting.

The Comparison in Fig. 14 is, in the general case, very time consuming because it requires the computation of 5000 FE solutions and thus, it would be obsolete in a practical application. Therefore, an alternative plausibility control is proposed requiring less computation time, based on the input variables $\xi_i(\theta)$. After the training process, the influence of the single input variables $\xi_i(\theta)$ is evaluated with the ANN function and compared with the FE solution. Therefore, only one random number ξ_i is considered in the KLE from Eq. (8), while the remaining random numbers are set to zero $\xi_j = 0,\ \forall\ j \neq i$. Thus, the random field from Eq. (8) reduces to

$$\widehat{w}(\boldsymbol{x}, \theta) = \xi_i(\theta) \cdot \sqrt{\lambda_i} \cdot \varphi_i(\boldsymbol{x}) \quad . \tag{22}$$

Starting with the first random number, ξ_1 is sampled on 13 equidistant sample points from -3 to 3 and the remaining random numbers are set constantly to zero $\xi_j = 0,\ \forall\ j \neq 1$. The first eigenvector $\varphi_1(\boldsymbol{x})$ is applied on the structure scaled with $\xi_1 \cdot \sqrt{\lambda_1}$ resulting in the response function for the critical buckling load factor, which is shown in Fig. 15 (left). The second response function is shown in Fig. 15 (right).

The same procedure is repeated for the first six eigenvectors $\varphi_i(\boldsymbol{x})$ of the covariance matrix. The ANN and FE solutions for the first six response functions and the cor-

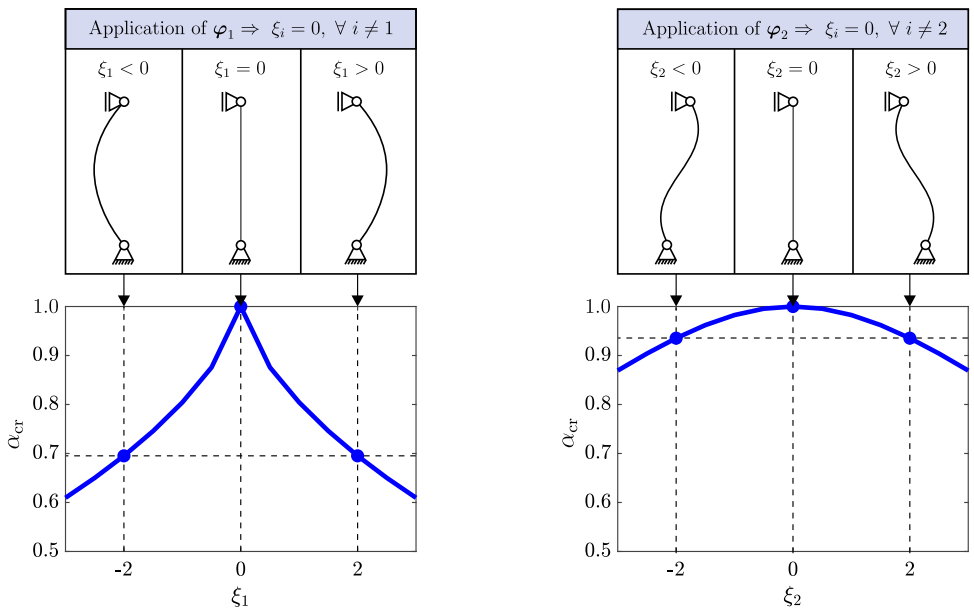

Fig. 15 First (left) and second (right) response function of the critical buckling factor α_{cr} of the column with $\ell_c = 200$ mm

responding eigenvectors are depicted in Figs. 16 and 17, respectively.

For the column, the application of an eigenvector as imperfection with positive or negative amplitude is equivalent. Therefore, all the response functions $\alpha_{\text{cr}}(\xi_i)$ are symmetric. For $\xi_i = 0$, the structure has no imperfections and thus, the response functions have the global maximum at $\alpha_{\text{cr}}(\xi_i = 0) = 1$. The characteristics can be further distinguished between even and odd numbered response functions:

$$\alpha_{\text{cr}}(\xi_{2k}) \quad \text{and} \quad \alpha_{\text{cr}}(\xi_{2k-1}) \,, \quad k \in \mathbb{N} \,. \tag{23}$$

It stands out, that the odd numbered response functions $\alpha_{\text{cr}}(\xi_{2k-1})$ in Fig 16 (left) have a sharp kink at the origin and higher influence on the critical buckling load factor α_{cr}. The even numbered response functions $\alpha_{\text{cr}}(\xi_{2k}),\ k \in \mathbb{N}$ in Fig 16 (right) correspond to a smooth curve and have low influence.

The reason for these particular characteristics of the response functions, is the shape of the eigenvectors of the covariance matrix $\varphi_i(\boldsymbol{x})$. Each eigenvector $\varphi_i(\boldsymbol{x})$ is multiplied with its affiliated random number $\xi_i(\theta)$ in the KLE, which are the input variables of the ANN. They have a sinusoidal shape and a number of local extrema equal to the number of eigenvalues i. The odd numbered eigenvectors have a local extremum in the middle of the column, which is unfavorable and therefore leads to a higher decrease of the buckling load.

This plausibility control is very simple, because in this example, the first eigenvector has the highest influence on the buckling load. In the following examples, the most important eigenvectors are within the first six eigenvectors. However, the plausibility control can be complex, e.g., in case of axial compressed cylinders, where it is not straight forward which eigenvector has the largest influence. In that case, the plausibility control has to be extended.

The computation of the response functions in Fig. 16 is very cheap. Considering the first six eigenvectors and evaluating each response function on 13 sample points, it costs $N_{\text{test}} = 6 \cdot 13 = 117$ FE solutions in total. This effort is negligible in comparison with a MCS of 5000 FE samples. This enables an efficient plausibility control of the trained ANN in practical applications. In Fig. 16, it is clearly visible, that the ANN function is able to learn the relationship between the single input variables ξ_i from the KLE and the buckling load.

4.2 Axially loaded plate

This example is a simply supported quadratic steel plate. The plate, shown in Fig. 18, has the thickness $t = 10\,\text{mm}$, Young's modulus $E = 210000\,\text{N/mm}^2$ and Poisson's ratio $\nu = 0.3$. The FE model consists of a 30×30 mesh, using 4

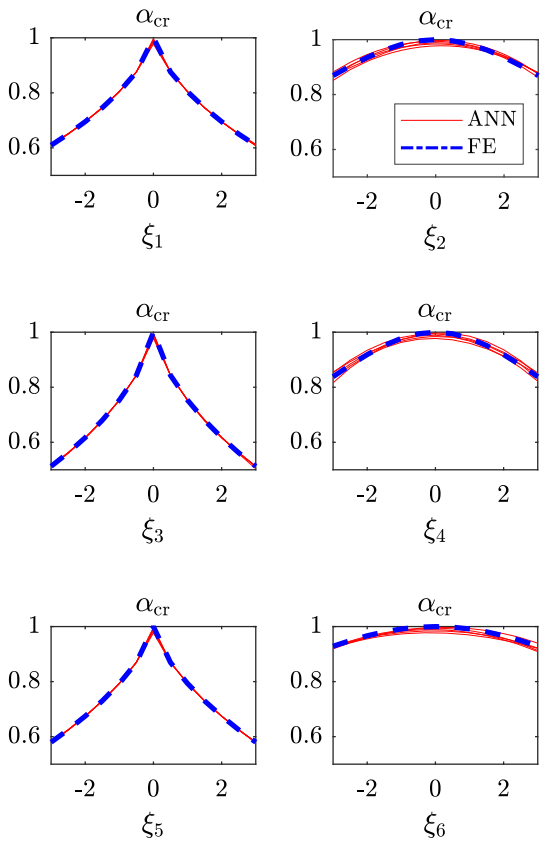

Fig. 16 ANN and FE solution for the first six response functions $\alpha_{\text{cr}}(\xi_i)$ of the column with $\ell_c = 200\,\text{mm}$ and a training set with 500 samples

node nonlinear shell elements with moderate rotations. All four edges are fixed perpendicular to the plane (BC $3 = u_3 = 0$) in x_3-direction. At $x_1 = 0$, the boundary condition (BC $1 = u_1 = 0$) is fixed in x_1-direction. The node at position $(x_1,x_2) = (0,0)$ is fixed in x_2-direction (BC $2 = u_2 = 0$). The plate is incrementally loaded with a distributed load p at $x_1 = 1000\,\text{mm}$.

The buckling load of a quadratic plate without imperfections is given in [55]

$$p_{\text{cr,perf,analyt}} = \frac{4\pi^2 D}{L^2} = 759.2\,\text{N/mm} \,, \tag{24}$$

where L is the length of the plate and D is the flexural rigidity

$$D = \frac{E \cdot t^3}{12(1-\nu^2)} \,. \tag{25}$$

The numerical buckling analysis of the structure without imperfections results in a critical load of $p_{\text{cr,perf}} = 758.73\,\text{N/mm}$ and a critical displacement of $u_{\text{cr}} = 0.361\,\text{mm}$. The critical buckling load factor α_{cr} is based on the numerical result of $p_{\text{cr,perf}}$. The load-displacement curves in Fig. 19 show a linear pre-buckling behavior and a bifurcation point for the plate without imperfection.

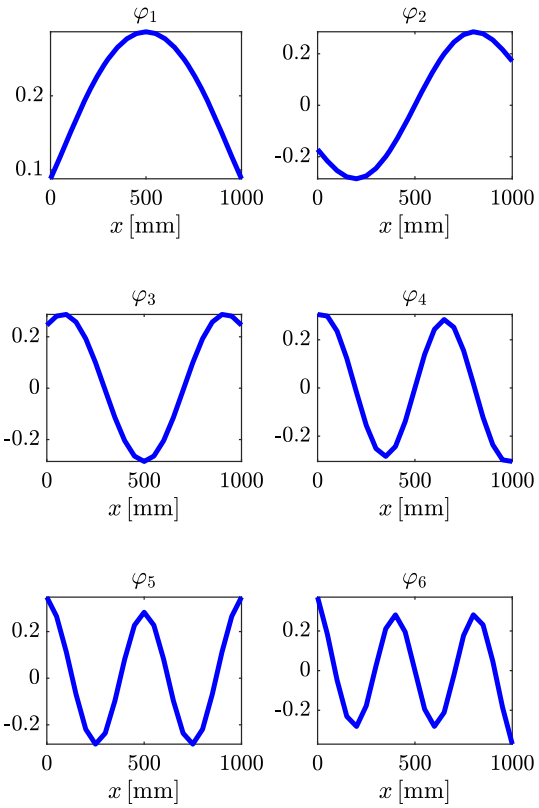

Fig. 17 First six eigenvectors of the covariance matrix of the column with $\ell_c = 200$ mm

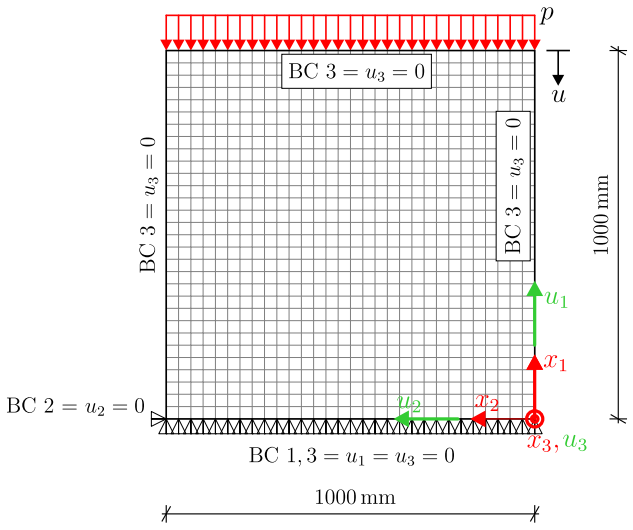

Fig. 18 FE mesh of the plate with 30 × 30 elements

In order to compute the post-buckling path, the first eigenmode with an amplitude of 1 mm is applied on the structure at the bifurcation point. The load-displacement curves for the imperfect structure are computed with a correlation length of $\ell_c = 500$ mm. Two realizations of random geometric imperfections $\widehat{w}$ that are applied on the plate are depicted in Fig. 20.

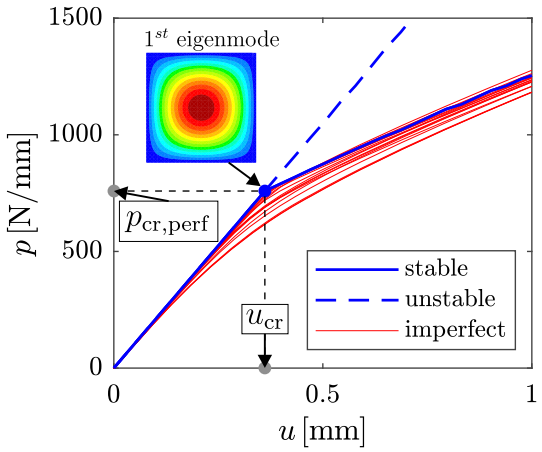

Fig. 19 Load displacement curves of the plate without and with imperfections for $\ell_c = 500$ mm

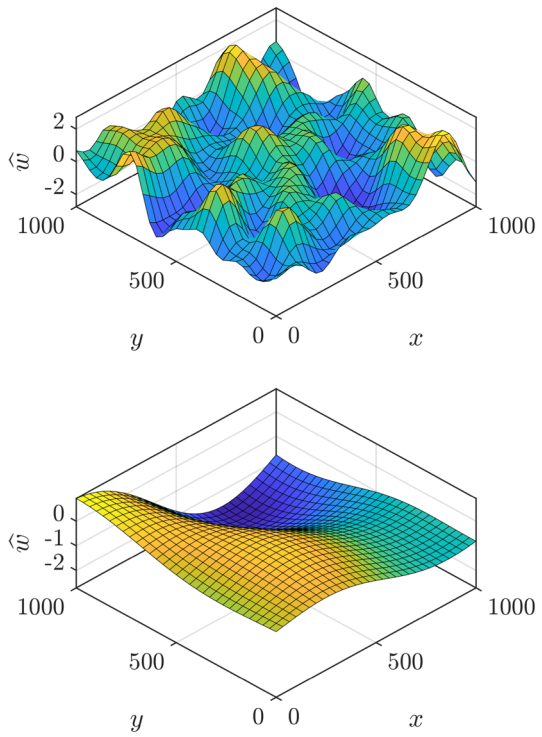

Fig. 20 Two exemplary realizations of random fields of the plate with $\ell_c = 100$ mm (top) and $\ell_c = 500$ mm (bottom)

With geometrical imperfections the bifurcation point disappears. Because the structure with geometrical imperfections has lower buckling loads, compared to the structure without imperfections, the critical buckling load factor α_{cr} is lower than 1, see Fig. 19. The KLE is truncated with a quality index of $Q = 0.99$. The number of investigated input variables N_{input} and training parameters N_{para} is summarized in Table 3.

The ANN training is carried out five times with five training sets of 500 samples. The training loss function, depicted

Table 3 Correlation lengths ℓ_c, number of input variables N_{input} and training parameters N_{para} for the plate

ℓ_c [mm]	100	200	300	400	500
N_{input}	177	51	26	17	12
N_{para}	2011	751	501	411	361

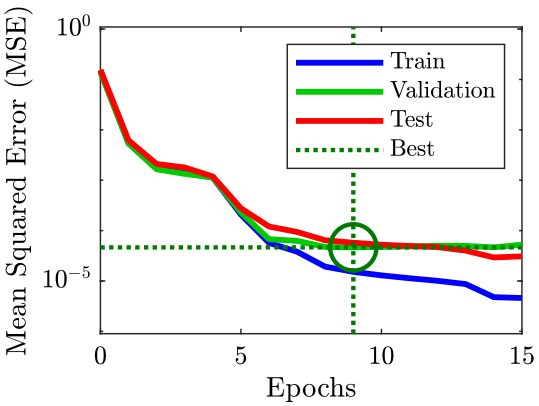

Fig. 21 Loss function evolution via training epochs of one ANN training process for the plate with $\ell_c = 500$ mm and a training set with 500 samples

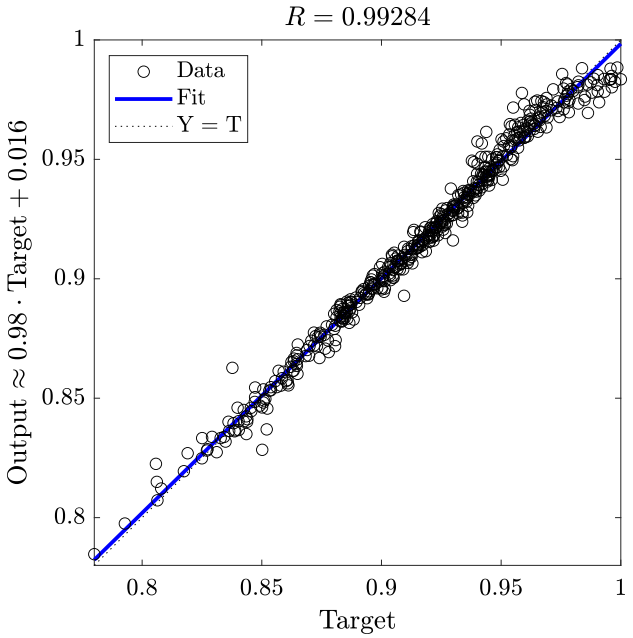

Fig. 22 Regression plot for training, testing and validation samples of one ANN training process for the plate with $\ell_c = 500$ mm and a training set with 500 samples

in Fig. 21, shows the MSE of the training, validation and testing sets in each epoch. The best validation performance is $4.65 \cdot 10^{-5}$ at epoch 8. The regression plot for training, validation and testing samples, is depicted in Fig. 22. The output-target points are scattering near the angle bisector, which means the ANN learned to predict the critical buckling load approximately.

Afterwards, the ANN function is tested on the first six response functions $\alpha_{cr}(\xi_i)$, shown in Fig. 23. Here, similar characteristics to the column example from the previous section are clearly visible. There are some response functions with a sharp kink and higher influence and some others resemble a smooth curve and have low influence.

The difference is, that in this example the characteristics does not alter between even and odd numbered response functions. The reason once again is the shape of the eigenvectors $\varphi_i(\boldsymbol{x})$ of the covariance matrix, which are depicted in Fig. 24.

The first, fifth and sixth eigenvector is symmetrical to the two center lines and thus, are favorable for the buckle formation. The second, third and fourth eigenvectors are symmetrical to the diagonals, which has negligible influence on the bucking load. The response functions with higher influence are also easier to train, because the neural network recognizes the higher importance of certain input variables. For the first, fifth and sixth response functions, the ANN solution does accurately approximate the FE solution. But for the second, third and fourth response functions, the ANN solution does not match the FE solution very well, see Fig 23.

The procedure is repeated for different amounts of samples in the training set and different correlation lengths. The cumulative distribution functions (CDFs) computed with 5000 MCS are presented in Fig. 25 for two different correlation lengths: $\ell_c = 200$ mm and $\ell_c = 500$ mm. The ANN solutions are produced with training sets of $N_{\text{train}} = 100,\ 500$ and 1000 samples. The ANN-CDFs are compared with the FE-CDFs with the same 5000 Monte Carlo samples. The trained ANN surrogate model shows a very good approximation for a correlation length of $\ell_c = 500$ mm and a training set with 500 samples. By using less samples $N_{\text{train}} = 100$ in the training set, the ANN approximation quality decreases, of course, especially because $N_{\text{train}} = 100 < N_{\text{para}} = 361$. At a lower correlation length of $\ell_c = 200$ mm the ANN has $N_{\text{para}} = 751$ training parameters but even with a training set with $N_{\text{train}} = 1000$ samples, one of the five ANN solutions does strongly diverge from the FE solution, which means that the ANN training is not robust.

For a more detailed comparison, the mean values μ, coefficient of variation CV and relative errors ε of the five ANN solutions are presented in Tables 4 and 5. The error does not decrease monotonically with the increase of samples in the training set N_{train} but fluctuates. In general, the ANN training is subject to a random weight initialization and thus, the predictions always inherit fluctuations. Therefore, increasing

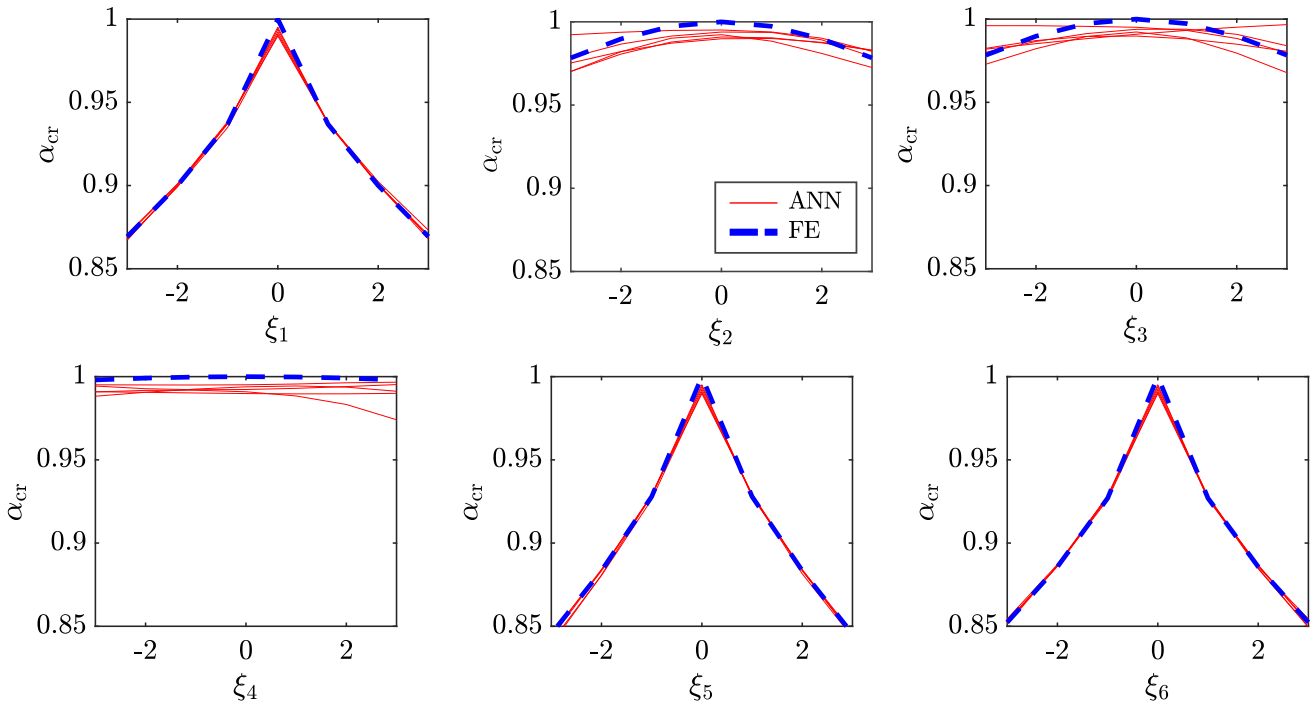

Fig. 23 First six response functions $\alpha_{cr}(\xi_i)$ of the plate with $\ell_c = 500\,\text{mm}$. Comparison between FE solution and five ANN solutions for five different training sets of 500 samples

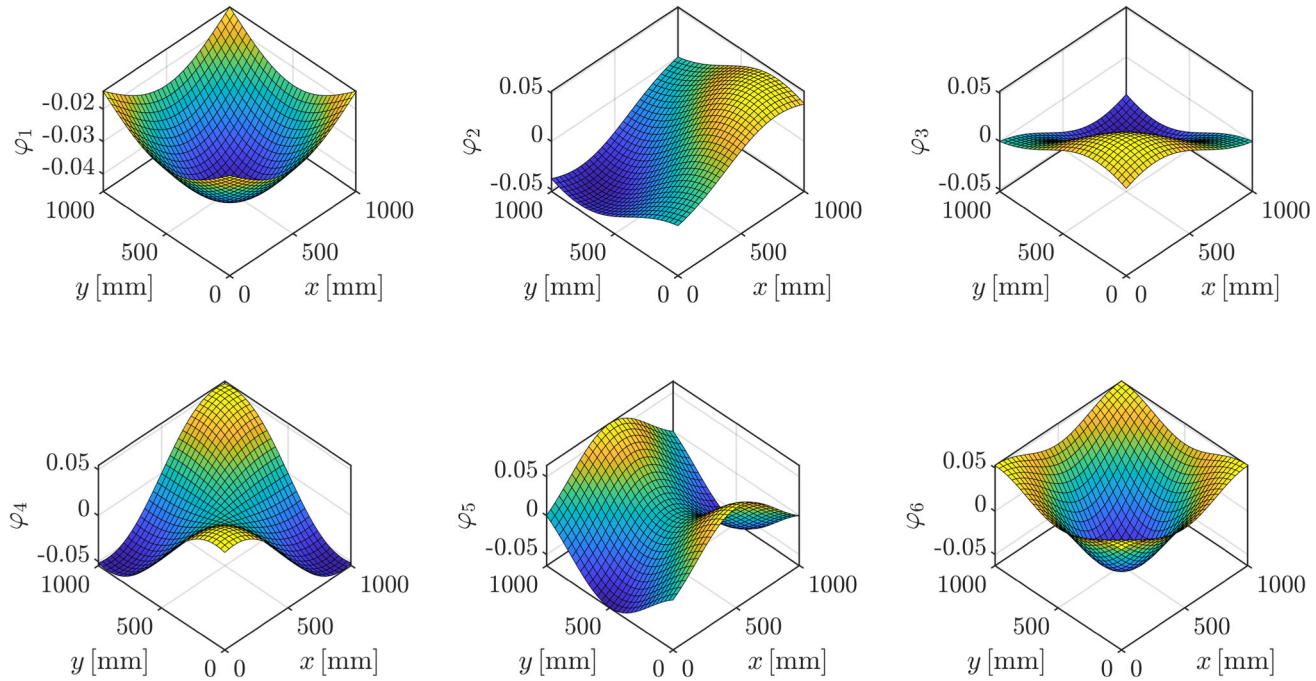

Fig. 24 First six eigenvectors of the covariance matrix of the plate for $\ell_c = 500\,\text{mm}$

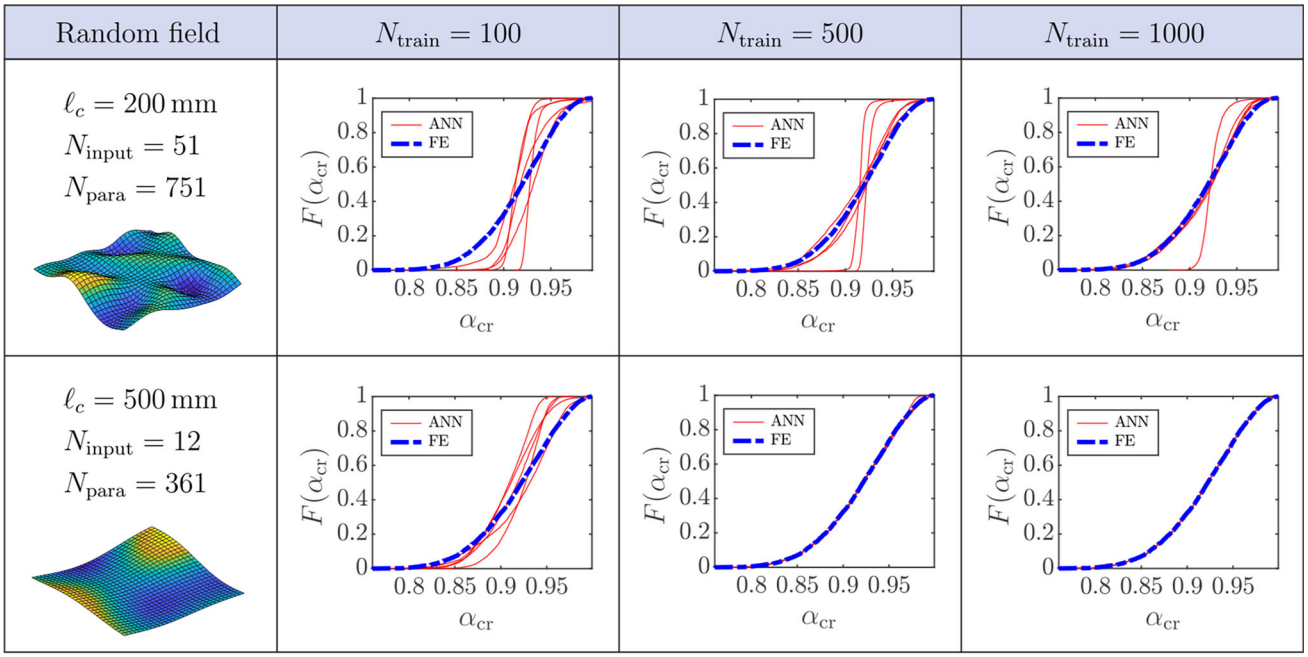

Fig. 25 Cumulative distribution functions for the plate with $\ell_c = 200$ and 500 mm, and $N_{\text{train}} = 100$, 500 and 1000. Comparison between FE solution and five ANN training sets

the samples in the training set N_{train}, will decrease the error with fluctuation. In order to measure the error of the ANN function and to summarize all results in one graph, the root mean square error (RMSE) is used.

$$\text{RMSE} = \sqrt{\frac{1}{N_{\text{mcs}}} \sum_{i=1}^{N_{\text{mcs}}} (\alpha_{\text{cr},i} - \widehat{\alpha}_{\text{cr},i})^2} \quad , \tag{26}$$

where α_{cr} is the FE solution and $\widehat{\alpha}_{\text{cr}}$ is the approximated solution, i.e. the ANN solution. Because each training procedure is repeated five times, the RMSE is represented as box-plot diagram in Fig. 26. The median of the box-plot is a measure for the accuracy, while the box-width and whiskers of the box-plot are measures for the robustness, where smaller boxes and whiskers means higher robustness. With increasing training set N_{train}, both the accuracy and the robustness tend to increase with possible fluctuations.

For higher correlation lengths, the error decrease is also higher. For low correlation lengths, the KLE requires more input variables and thus more input neurons in the ANN. Therefore, if the samples in the training set are kept constant, the ANN error increases for lower correlation lengths. For a given accuracy, the ANN of a lower correlation length requires more samples in the training set, compared to a higher correlation length. In order to compare the ANN and FE computation time, an error tolerance of tol = 0.015 has been chosen, which is depicted in Fig. 26 as dashed line. For each correlation length ℓ_c the best ANN training settings for

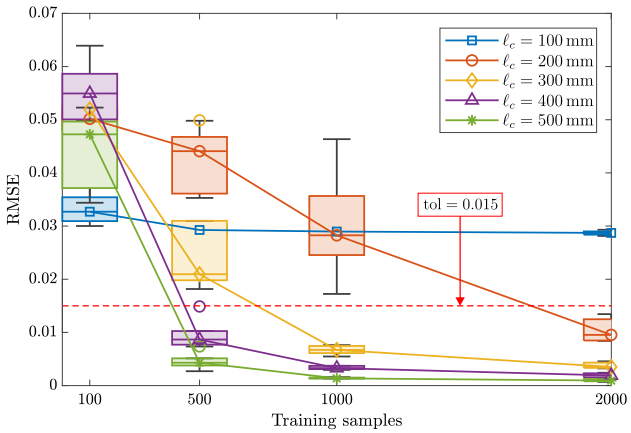

Fig. 26 RMSE and selected tolerance value of the ANN for different correlation lengths ℓ_c [mm] in a box plot diagram for the plate

RMSE $<$ tol $= 0.015$ are used to calculate the required ANN computation time t_{ANN}. The total ANN computation time consists of the training time and the time for generating the training, testing and validation samples with the FE buckling analysis.

The ratio between FE and ANN computation time $t_{\text{FE}}/t_{\text{ANN}}$, i.e. the speedup factor, is depicted in Fig 27. The total FE computation time consists of 5000 FE-MCS samples. For the correlation length of $\ell_c = 100$ mm the RMSE is higher than the error tolerance for all investigated training sets and therefore, it is not included in Fig. 27.

Table 4 Mean value μ of the critical buckling load factor α_{cr} for the plate. Reference FE solution μ_{FE}, five ANN training results $\mu_{ANN,i}$ and corresponding percentage errors ε_i [%]

ℓ_c [mm]	μ_{FE}	N_{train}	$\mu_{ANN,1}$	ε_1[%]	$\mu_{ANN,2}$	ε_2[%]	$\mu_{ANN,3}$	ε_3[%]	$\mu_{ANN,4}$	ε_4[%]	$\mu_{ANN,5}$	ε_5[%]
200	0.9168	100	0.9242	0.80	0.9306	1.50	0.9219	0.56	0.9232	0.70	0.9393	2.46
		500	0.9127	0.45	0.9174	0.06	0.9168	0.00	0.9106	0.68	0.9122	0.50
		1000	0.9163	0.06	0.9168	0.00	0.9184	0.17	0.9164	0.05	0.9173	0.05
		2000	0.9156	0.14	0.9160	0.09	0.9169	0.01	0.9171	0.03	0.9170	0.02
500	0.9184	100	0.9214	0.32	0.9130	0.59	0.9167	0.19	0.9150	0.37	0.9221	0.41
		500	0.9187	0.03	0.9189	0.06	0.9185	0.01	0.9187	0.03	0.9189	0.05
		1000	0.9186	0.02	0.9186	0.02	0.9186	0.02	0.9186	0.02	0.9186	0.02
		2000	0.9185	0.02	0.9185	0.01	0.9186	0.02	0.9186	0.02	0.9186	0.02

Table 5 Coefficient of variation CV [%] of the critical buckling load factor α_{cr} for the plate. Reference FE solution CV_{FE} [%], five ANN training results $CV_{ANN,i}$ [%] and corresponding percentage errors ε_i [%]

ℓ_c [mm]	CV_{FE}	N_{train}	$CV_{ANN,1}$	ε_1	$CV_{ANN,2}$	ε_2	$CV_{ANN,3}$	ε_3	$CV_{ANN,4}$	ε_4	$CV_{ANN,5}$	ε_5
200	4.18	100	3.62	13.23	1.67	60.09	2.20	47.19	1.30	68.78	3.21	22.93
		500	2.12	49.16	3.80	8.94	0.82	80.37	0.98	76.61	0.96	76.90
		1000	4.04	3.15	3.83	8.19	3.87	7.25	4.15	0.50	4.14	0.87
		2000	4.02	3.75	4.16	0.30	4.12	1.35	4.16	0.43	4.21	0.75
500	0.0466	100	3.95	15.22	4.22	9.51	2.24	51.88	4.14	11.16	3.06	34.33
		500	4.64	0.37	4.63	0.53	4.61	1.06	4.61	1.01	4.67	0.19
		1000	4.63	0.70	4.61	1.01	4.63	0.60	4.61	0.97	4.62	0.79
		2000	4.63	0.63	4.63	0.63	4.63	0.68	4.62	0.80	4.62	0.74

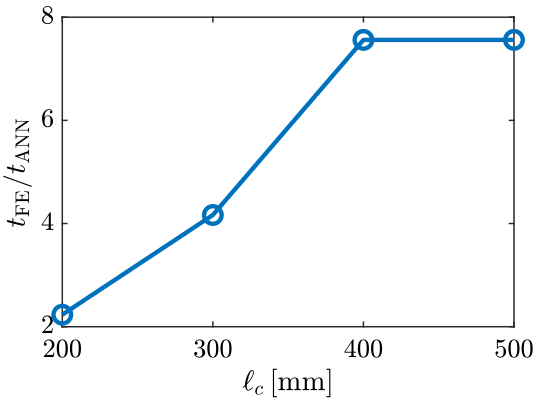

Fig. 27 Speedup factor for the plate: ratio between FE and ANN computation time t_{FE}/t_{ANN} via correlation length ℓ_c

This example shows, that the ANN is able to predict the probability distribution for the plate with significant time saving, which will further increase if more than 5000 MCS samples are required to access the probabilistic quantity of interest, e.g., low failure probabilities. However, the correlation length ℓ_c has an important influence on the number of input variables and thus, on the training performance. Low correlation lengths lead to a very difficult training process and even insufficient results for the presented training sets.

Table 6 Correlation lengths ℓ_c, number of input variables N_{input} and training parameters N_{para} of the cylindrical shell segment

ℓ_c [mm]	100	150	200	250
N_{input}	52	26	17	12
N_{para}	761	501	411	361

For the same correlation length $\ell_c = 200$ mm, the CV of the buckling load of the plate is much smaller, compared to the column example, even though all random fields are modelled with the same mean value $\mu = 0$ and standard deviation $\sigma = 1$. This shows, that the variation of the buckling load depends on the structure type and boundary conditions.

4.3 Cylindrical shell segment

A more particular structure with different buckling behavior is presented in the next example, where a cylindrical shell segment is investigated. It is taken from [46] and depicted in Fig. 28. The shell is loaded in the center in the negative z-direction with the load P and the displacement w_c in negative z-direction is measured for the load-displacement curve. The shell is simply supported on the two lateral edges. The FE model consists of a 30×30 mesh, using 4 node nonlinear shell elements with moderate rotations.

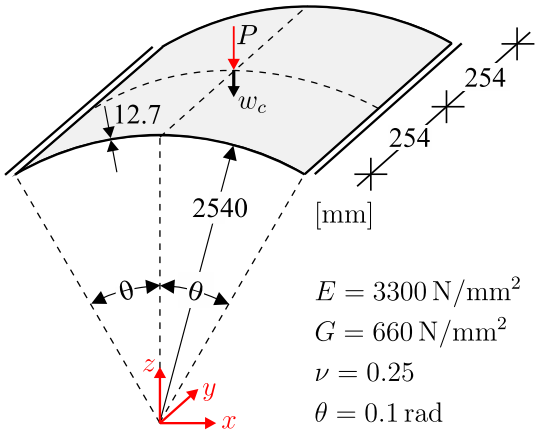

Fig. 28 Cylindrical shell segment with 30×30 elements

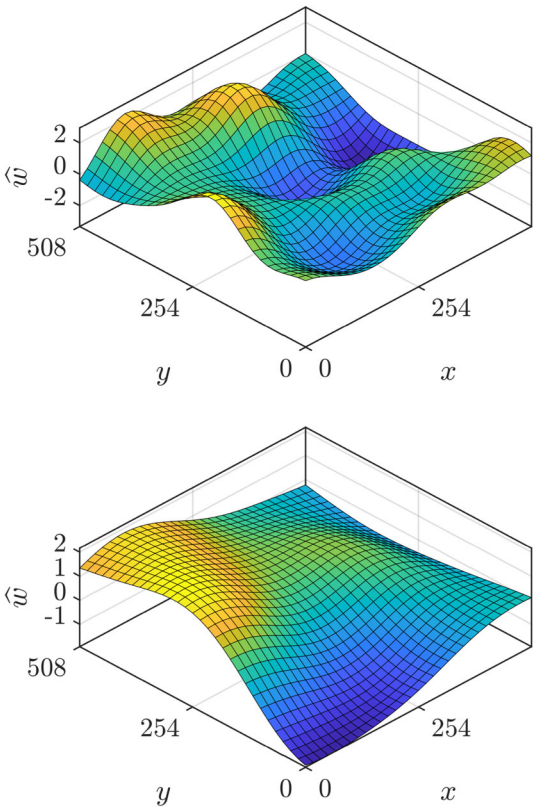

Fig. 29 Two exemplary unrolled random field realizations for the cylindrical shell segment with $\ell_c = 100\,\mathrm{mm}$ (top) and $\ell_c = 200\,\mathrm{mm}$ (bottom)

Because the cylindrical shell segment is a curved structure, the radial imperfections are realized on the unrolled surface. Two examples of unrolled random field realizations $\widehat{w}$ for the cylindrical shell segment with $\ell_c = 100\,\mathrm{mm}$ and $\ell_c = 200\,\mathrm{mm}$ are shown in Fig. 29.

The KLE is truncated with a quality index of $Q = 0.99$. The number of input variables N_{input} and the number of training parameters N_{para} used in this example are summarized in Table 6.

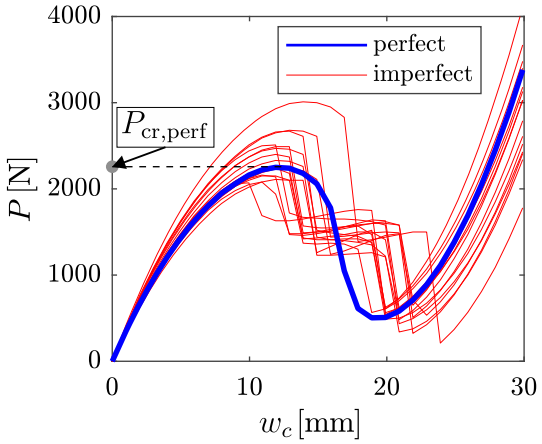

Fig. 30 Load displacement curves of the cylindrical shell segment without and with imperfections for $\ell_c = 200\,\mathrm{mm}$

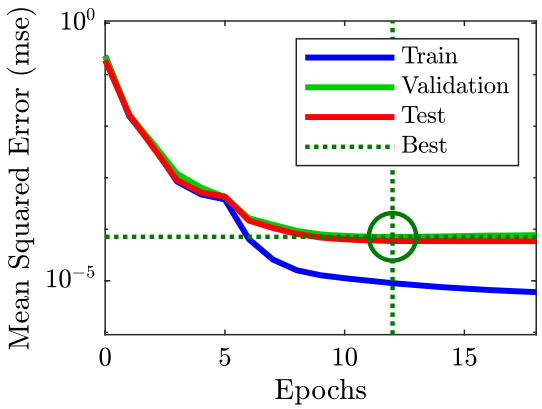

Fig. 31 Loss function evolution of one ANN training process for the cylindrical shell segment with $\ell_c = 200\,\mathrm{mm}$ and a training set of 500 samples

The load-displacement curve in Fig. 30 is non-linear and has a limit point at $P_{\mathrm{cr,perf}} = 2249.79\,\mathrm{N}$ for the structure without imperfections. The load-displacement curves with geometrical imperfections calculated for $\ell_c = 200\,\mathrm{mm}$ are shown in Fig. 30. Despite imperfections they still have a limit point, beyond which two consecutive load decreases occur. Then, the load-displacement curves of the structure with and without imperfections continue approximately parallel. The buckling load of the imperfect structure can even be higher than without imperfections, which means the critical buckling load factor can be higher than one.

The ANN training is carried out five times with a random field with $\ell_c = 200\,\mathrm{mm}$ and a training set with $N_{\mathrm{train}} = 500$ samples. The training loss function, depicted in Fig. 31, shows the MSE of the training, validation and testing sets in each epoch. The best validation performance is $7.13 \cdot 10^{-5}$ at epoch 12. The regression plot for training, validation and test-

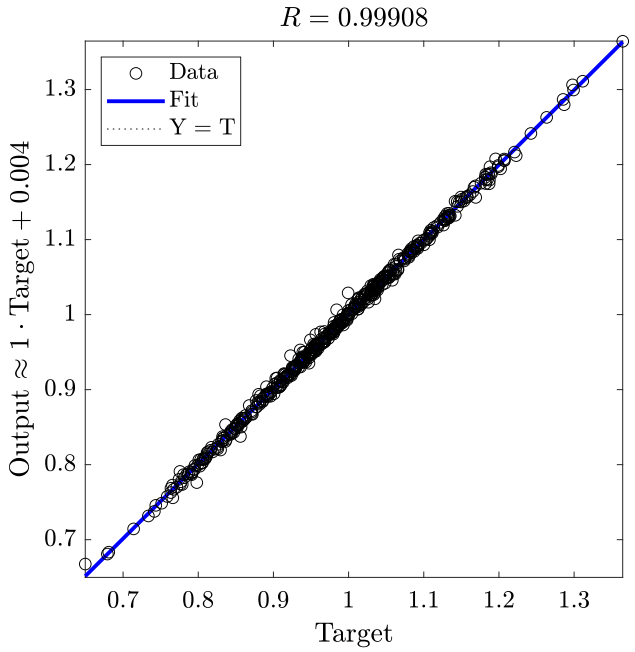

Fig. 32 Regression plot for training, testing and validation samples of one ANN training process for the cylindrical shell segment with $\ell_c = 200\,\text{mm}$ and a training set with 500 samples

ing samples, is depicted in Fig. 32. The output-target points are very close to the angle bisector, which means that the ANN learned to predict the critical buckling load accurately.

After the ANN training with the training set with $N_{\text{train}} = 500$ samples, the ANN surrogate model is tested on the first six response functions $\alpha_{cr}(\xi_i)$, shown in Fig. 33. The affiliated eigenvectors $\varphi_i(\boldsymbol{x})$ of the covariance matrix are presented in Fig. 34. The first and the fifth eigenvector are able to enforce the upward curvature of the shell without imperfection, which offers a higher arch support effect for the downward load and therefore leads to higher buckling loads.

The corresponding response functions $\alpha_{cr}(\xi_i)$ are almost linear with a positive gradient reaching values greater than one. The second, third, fourth and sixth eigenvectors are not able to offer this effect and therefore the corresponding response function graphs $\alpha_{cr}(\xi_i)$ are almost a horizontal line at the value of $\alpha_{\text{cr}} = 1$, which means they have nearly no influence on the buckling load. Compared to the previous examples, not all response functions are symmetrical, some of them are monotonous and also none of them has a kink.

The MCS is performed with $N_{\text{mcs}} = 5000$ samples of the ANN solution. The procedure is repeated investigating different correlation lengths and different training sets with five training process repetitions. The resulting CDFs are depicted in Fig. 35. For the correlation length of $\ell_c = 200\,\text{mm}$ and training sets of 500 to 1000 samples, the probability distribution computed by the ANN surrogate model is a very accurate approximation of the FE solution, as there is no visible error. Lowering the training set to $N_{\text{train}} = 100 < N_{\text{para}} = 411$, the ANN error is clearly visible.

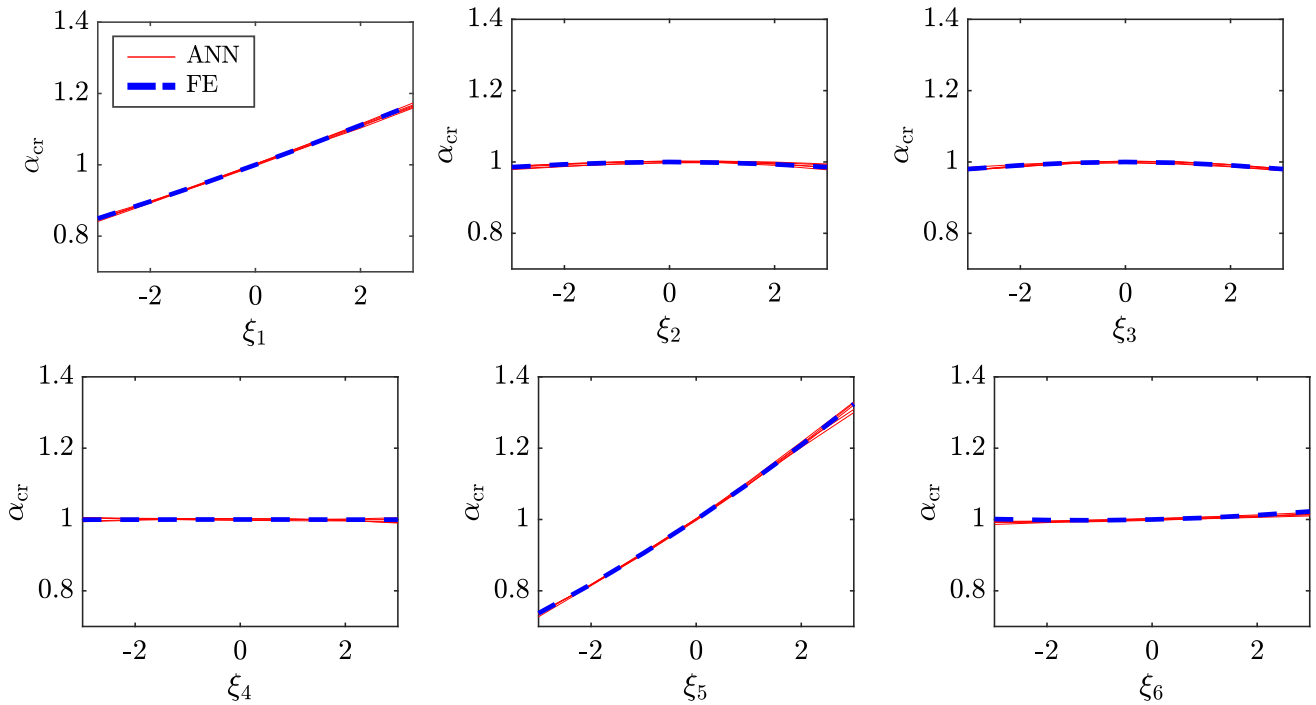

Fig. 33 First six response functions $\alpha_{\text{cr}}(\xi_i)$ of the cylindrical shell segment with $\ell_c = 200\,\text{mm}$. Comparison between FE solution and five ANN solutions for five different training sets of 500 samples

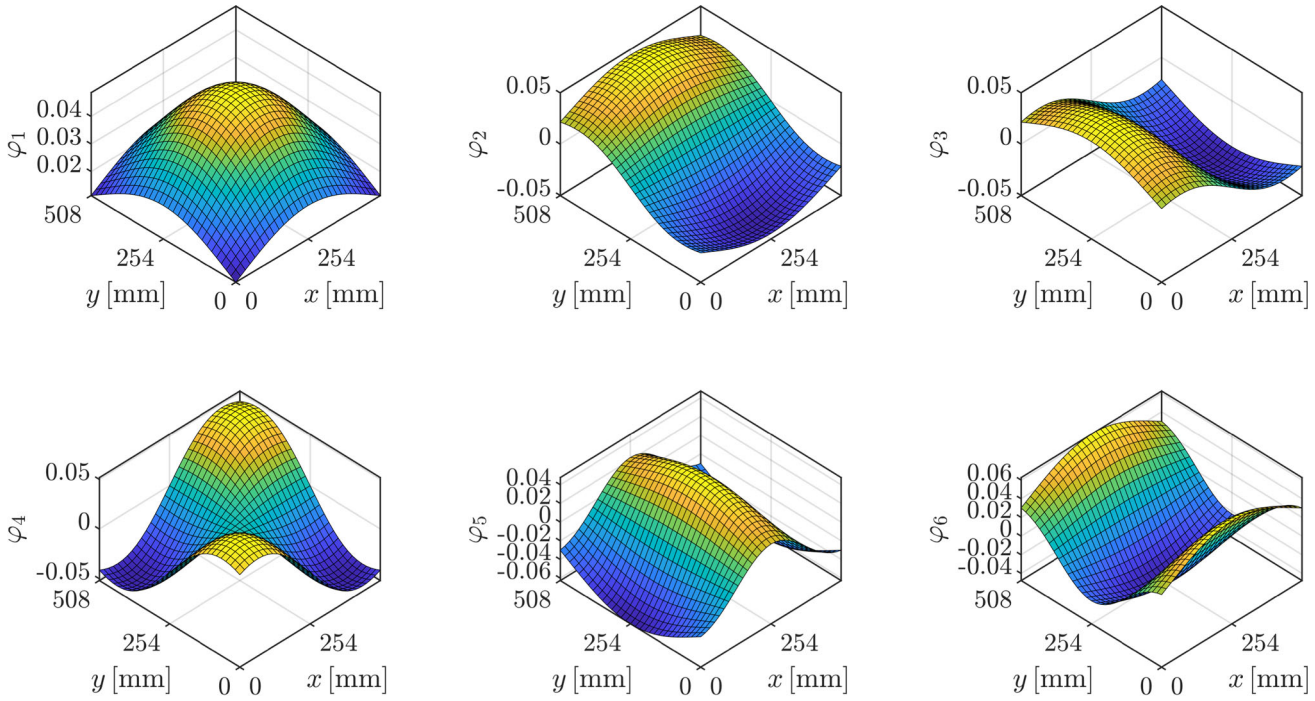

Fig. 34 First six eigenvectors of the covariance matrix of the cylindrical shell segment for $\ell_c = 200\,\text{mm}$

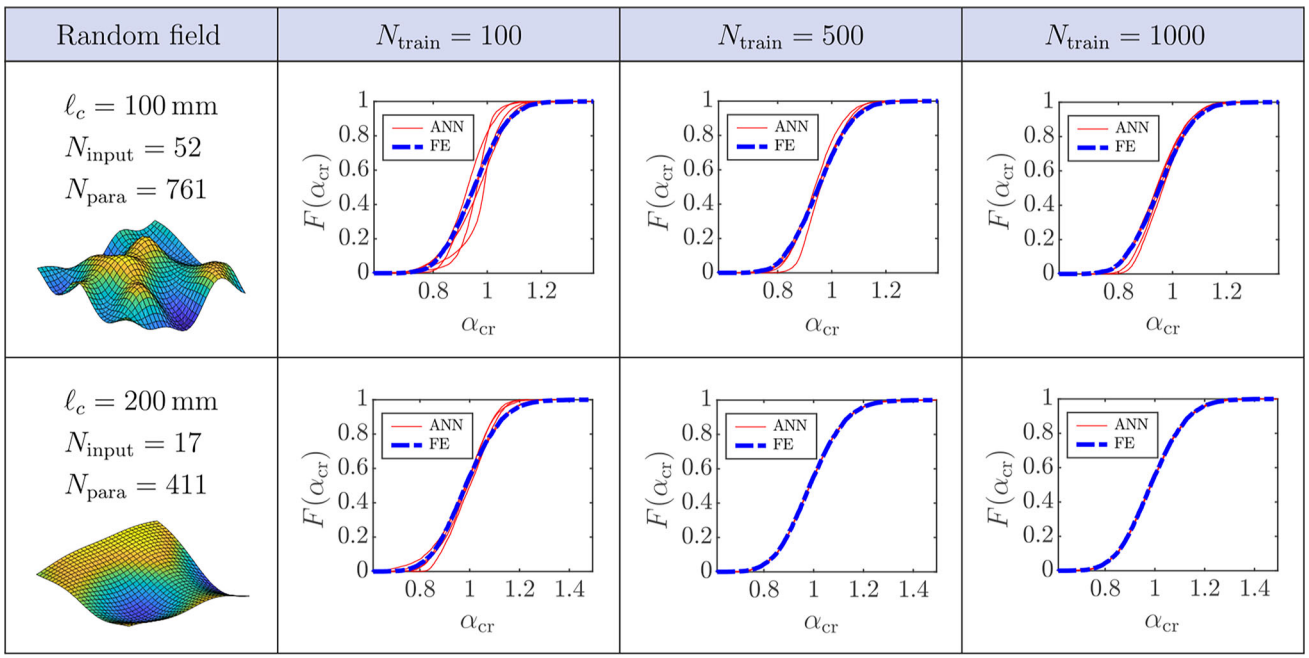

Fig. 35 Cumulative distribution functions for the cylindrical shell segment with $\ell_c = 100$ and 200 mm and $N_{\text{train}} = 100$, 500 and 1000 training sets. Comparison between FE solution and five ANN training sets

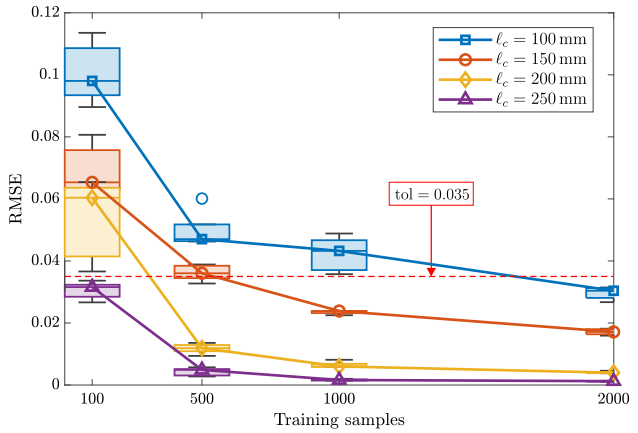

Fig. 36 RMSE and selected tolerance value of the ANN for different correlation lengths ℓ_c [mm] in a box plot diagram for the cylindrical shell segment

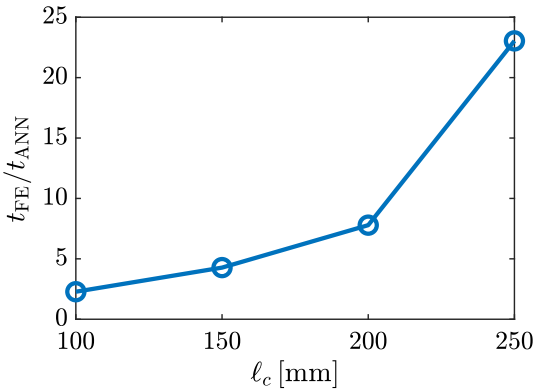

Fig. 37 Speedup factor for the cylindrical shell segment: ratio between FE and ANN computation time $t_{\mathrm{FE}}/t_{\mathrm{ANN}}$ via correlation length ℓ_c

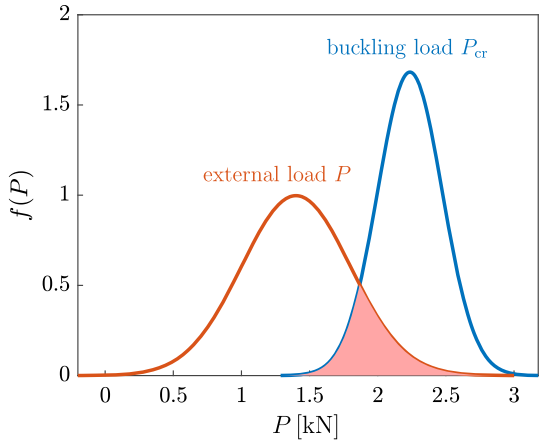

Fig. 38 PDF of the buckling load of the cylindrical shell segment based on 10^5 FE-MCS with $\ell_c = 250$ mm and PDF of a variable external load of $P \sim \mathcal{N}(1.4, 0.4)$ kN

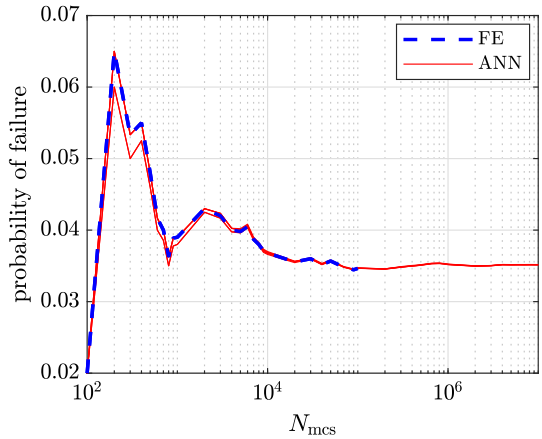

Fig. 39 FE and ANN solution of the probability of failure with increasing amount of Monte Carlo samples for the cylindrical shell segment with $\ell_c = 250$ mm, a training set of 2000 samples and an external load of $P \sim \mathcal{N}(1.4, 0.4)$ kN

For a lower correlation length of $\ell_c = 100$ mm the ANN training becomes highly demanding. Even at $N_{\mathrm{train}} = 1000 > N\mathrm{para} = 761$ the surrogate model shows significant errors.

The mean values μ, coefficient of variation CV and relative errors ε of the five ANN solutions are presented in Tables 7 and 8. The error measurement is summarized with the RMSE in a box-plot diagram in Fig. 36.

The RMSE of the ANN for all investigated correlation lengths have a noticeable decrease with increasing number of samples of the training set N_{train}. However, with lower correlation lengths ℓ_c the training is more difficult and the error is higher.

In order to compare the ANN and FE computation time, an error tolerance of tol $= 0.035$ has been chosen, which is depicted in Fig. 36 as dashed line. For each correlation length ℓ_c, the best ANN training settings for RMSE $<$ tol $= 0.035$ are used to calculate the required ANN computation time t_{ANN}.

The ratio between FE and ANN computation time $t_{\mathrm{FE}}/t_{\mathrm{ANN}}$, i.e. the speedup factor, is depicted in Fig. 37. The total FE computation time consists of 5000 FE-MCS samples.

The shell structure shows similar results compared to the plate example. The training performance depends not only on the training set, but also on the correlation length.

In order to further demonstrate the computational benefit, the probability of failure P_f is calculated as stochastic quantity of interest for a given external load $P \sim \mathcal{N}(1.4, 0.4)$ kN. The probability of failure is defined as the probability that the buckling load is smaller than the external load: $P_f = Prob.(P_{\mathrm{cr}} < P)$. For the correlation length $\ell_c = 250$ mm an MCS with 10^5 simulations is computed for the buckling load P_{cr} and the external load P. The corresponding PDFs are plotted in Fig. 38. For a gradually increasing number of simulations, the probability of failure is calculated with the FE and ANN solution based on a training set of 2000 samples

Table 7 Mean value μ of the critical buckling load factor α_{cr} for the cylindrical shell segment. Reference FE solution μ_{FE}, five ANN training results $\mu_{ANN,i}$ and corresponding percentage errors ε_i [%]

ℓ_c [mm]	μ_{FE}	N_{train}	$\mu_{ANN,1}$	ε_1[%]	$\mu_{ANN,2}$	ε_2[%]	$\mu_{ANN,3}$	ε_3[%]	$\mu_{ANN,4}$	ε_4[%]	$\mu_{ANN,5}$	ε_5[%]
100	0.9530	100	0.9749	2.30	0.9606	0.80	0.9604	0.77	0.9236	3.08	0.9548	0.19
		500	0.9511	0.20	0.9679	1.56	0.9527	0.03	0.9506	0.25	0.9408	1.27
		1000	0.9534	0.04	0.9460	0.73	0.9703	1.82	0.9428	1.07	0.9633	1.09
		2000	0.9535	0.05	0.9493	0.39	0.9530	0.00	0.9526	0.04	0.9531	0.01
200	0.9909	100	0.9894	0.15	0.9886	0.23	0.9706	2.05	1.0057	1.50	0.9826	0.84
		500	0.9899	0.10	0.9902	0.08	0.9903	0.07	0.9882	0.27	0.9910	0.01
		1000	0.9889	0.20	0.9897	0.12	0.9896	0.13	0.9893	0.16	0.9898	0.11
		2000	0.9891	0.18	0.9895	0.14	0.9893	0.16	0.9895	0.14	0.9894	0.15

Table 8 Coefficient of variation CV [%] of the critical buckling load factor α_{cr} for the cylindrical shell segment. Reference FE solution CV_{FE} [%], five ANN training results $CV_{ANN,i}$ [%] and corresponding percentage errors ε_i [%]

ℓ_c [mm]	CV_{FE}	N_{train}	$CV_{ANN,1}$	ε_1	$CV_{ANN,2}$	ε_2	$CV_{ANN,3}$	ε_3	$CV_{ANN,4}$	ε_4	$CV_{ANN,5}$	ε_5
100	10.45	100	8.35	20.08	10.34	1.07	9.62	7.94	9.18	12.19	6.87	34.27
		500	10.22	2.25	7.45	28.66	9.51	9.01	10.42	0.28	8.85	15.33
		1000	10.12	3.20	9.61	8.09	8.42	19.43	9.75	6.76	8.87	15.14
		2000	10.53	0.69	10.31	1.35	10.25	1.99	10.63	1.68	10.56	1.00
200	11.62	100	11.16	4.03	9.91	14.72	11.25	3.21	9.73	16.34	9.99	14.06
		500	11.81	1.62	11.50	1.07	11.74	0.99	11.59	0.26	11.68	0.48
		1000	11.73	0.87	11.68	0.52	11.63	0.03	11.67	0.41	11.64	0.11
		2000	11.71	0.75	11.71	0.76	11.69	0.59	11.72	0.81	11.72	0.82

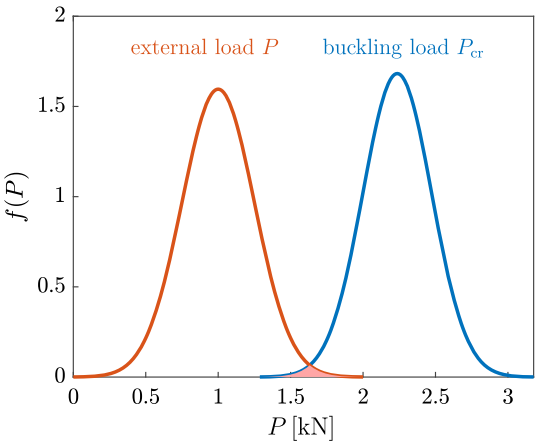

Fig. 40 PDF of the shells buckling load of the cylindrical shell segment based on 10^5 FE-MCS with $\ell_c = 250$ mm and PDF of a variable external load of $P \sim \mathcal{N}(1.0, 0.25)$ kN

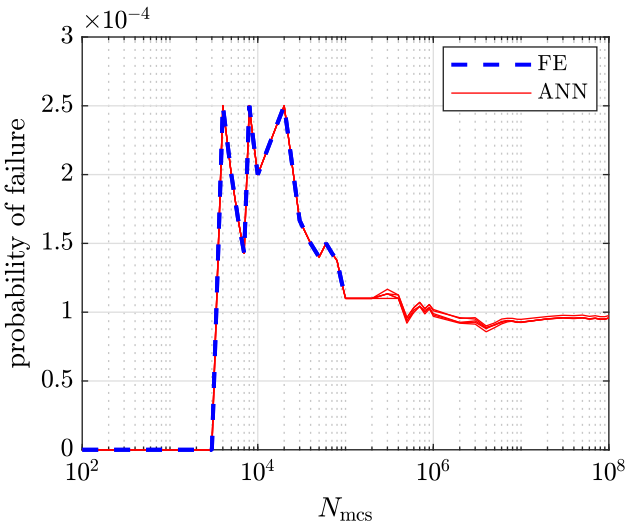

Fig. 41 FE and ANN solution of the probability of failure with increasing amount of Monte Carlo samples for the cylindrical shell segment with $\ell_c = 250$ mm, a training set of 2000 samples and an external load of $P \sim \mathcal{N}(1.0, 0.25)$ kN

and is plotted in Fig. 39. The FE-MCS is computed with 10^5 simulations and the ANN-MCS is computed with up to 10^7 simulations to show the convergence (Fig. 39). It is visible, that the probability of failure is stabilized at $P_f = 0.035$. In order to show the convergence for a lower probability of failure, the same calculation is repeated for an external load of $P \sim \mathcal{N}(1.0, 0.25)$ kN, with the corresponding PDFs presented in Fig. 40. The probability of failure with up to 10^8 ANN-MCS samples and 10^5 FE-MCS samples is depicted in Fig. 41 and is stabilized at $P_f = 9.50 \cdot 10^{-5}$. Compared to the previous calculation, the convergence is

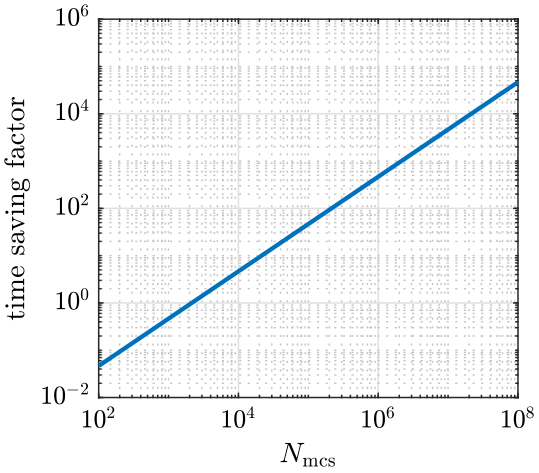

Fig. 42 ANN time saving factor based on the number of Monte Carlo samples for the cylindrical shell segment with $\ell_c = 250\,\mathrm{mm}$ and a training set of 2000 samples

slower, because the probability of failure is lower. This shows how the Monte Carlo convergence depends on the stochastic quantity of interest. The advantage in using the ANN, provided a successful training process, is that any desired amount of samples can be produced without further computational effort. This means, that the ANN benefit increases with increasing number of simulations. The ANN results in Figs. 39 and 41 are plotted for five training process repetitions, showing that the ANN surrogate model is not only very accurate, but also robust.

For the last example of the shell with $\ell_c = 250\,\mathrm{mm}$ and a training set of 2000 samples, the time saving factor with respect to the number of simulations is plotted in Fig. 42. Based on how many samples are used, the time saving factor can be determined from Fig. 42. The calculation of the time saving factor includes the computation time of the samples in the training set. Thus, for a number of Monte Carlo samples lower than the number of samples used in the training set, the time saving factor is lower than one. The calculation with 10^8 samples yields a time saving factor ≈ 46577. It is evident, that the calculation of a low probability demands high numbers of Monte Carlo samples. The reliability analysis in civil engineering requests the probability of failure to be lower than $10^{-5} - 10^{-3}$ depending on the structures consequence class [17]. In this context, the presented method offers significant time savings.

5 Conclusion and outlook

A new approach of ANN surrogate modeling for geometrical imperfections with random fields in buckling analysis has been presented. The aim of this method is the reduction of the Monte Carlo Simulations computation time. The novelty of this work is the use of the random field's variables $\xi_i(\theta)$ as ANN input. The method has been applied to three different structures in order to demonstrate that the ANN is able to learn different relationships between the input variables $\xi_i(\theta)$ and the buckling load. It has been shown, that the surrogate model can efficiently predict the buckling loads of imperfect structures with significant time savings. The eigenvectors $\boldsymbol{\varphi}_i$ of the covariance matrix have different sensitivities on the buckling load depending on their shape. Some of them have almost no influence on the output and can potentially be neglected. Therefore, the presented method can be enhanced in future studies with a sensitivity analysis of single eigenvectors of the covariance matrix on the buckling load. The idea is to eliminate nonsensitive eigenvectors, in order to reduce the number of input variables.

In general, the ANN time saving factor varies depending on the stochastic quantity of interest and the correlation length. If one is only interested in mean value and variance of the buckling load, few samples can be enough and the ANN benefit is negligible. However, in a probabilistic safety assessment, a low probability of failure must be guaranteed, which requires a very high number of samples. In that case, the ANN benefit becomes even more significant.

It is important to notice, that the performance of the presented surrogate model depends on the random field's correlation length ℓ_c. In order to further validate the presented method with realistic correlation lengths, real measurements are of crucial importance. Future works will aim on the ANN training on realistic random fields derived from surface measurements, which are very rare to find in literature. Often, the available data is insufficient because only a small number of specimens are measured. In this case the correlation length ℓ_c can be interpreted as interval or fuzzy variable considering epistemic uncertainty. In that case, the computation procedure consists of a two loops algorithm, where the inner loop is the MCS and the outer loop is the interval or fuzzy analysis. Therefore, the ANN training procedure has to be enhanced including the correlation length ℓ_c as input variable in the ANN. One of the problems in this intent, is that the number of input neurons may vary during one training process which is not possible in common neural networks. One obvious way to avoid this issue, is to use random fields with quality index $Q = 1$ so that the number of input variables is constantly equal to the random field nodes. However, this comes with a high number of input variables and can decrease the ANN training performance, which has to be investigated.

The authors main project is the design optimization of shell structures with geometrical imperfections. This introduces design variables to the calculation process, which can be, for example, the fiber angles in layered composite structures or stringers for stiffened shells. Together with fuzzy or interval variables, as for example the correlation length, the

complete computation model consists of the following three levels with different input variable types:

- *Stochastic analysis*: random numbers $\xi_i(\theta)$
- *Interval/fuzzy analysis*: correlation length ℓ_c
- *Design optimization*: fiber angles, stringer setup

The variables in this list are only a possible example. Even more variables can be added. In future works, the surrogate model will include these three different variable types in a multi-loop algorithm.

In the framework of artificial intelligence methods, a large variety of different neural networks are established as surrogate models. The presented method can be applied on alternative neural network types.

In further studies, the whole concept shall be tested on other structure types. Especially full cylindrical shells are of particular interest because of their high sensitivity to buckling failure under geometrical imperfections. The high number of required FE nodes, and thus the high number of input variables $\xi_i(\theta)$ for cylinders are challenging in computation time, both for the FE solution and the ANN training. Therefore, the development of an efficient surrogate model for random fields in buckling analysis of cylindrical shells is still demanding.

Acknowledgements Financial support was provided by the deutsche Forschungsgemeinschaft (DFG, German Research Foundation) in the framework of project 511267658. This support is gratefully acknowledged.

References

1. Robertson A (1928) The strength of tubular struts. Proc Royal Soc Lond Ser A, Contain Pap Math Phys Charact 121(788):558–585. https://doi.org/10.1098/rspa.1928.0219
2. Koiter WT (1945) On the stability of elastic equilibrium. PhD thesis, Polytechnic Institute Delft, English Translation (1967): NASA TT F-10
3. Donnell LH, Wan CC (1950) Effect of imperfections on buckling of thin cylinders and columns under axial compression. J Appl Mech 17(1):73–83. https://doi.org/10.1115/1.4010060
4. NASA (1968) Buckling of thin-walled circular cylinders. NASA SP-8007
5. Budiansky B, Hutchinson JW (1966) A survey of some buckling problems. AIAA J 4(9):1505–1510
6. Bolotin VV (1957) Statistical Methods in the Nonlinear Theory of Elastic Shells: Presented at a Seminar in the Institute of Mechanics of the Academy of Sciences USSR on 3:1962
7. Bolotin VV (1967) Statistical aspects in the theory of structural stability. In: Dynamic Stability of Structures, pp 67–81. https://doi.org/10.1016/B978-1-4831-9821-7.50009-0
8. Roorda J (1969) Some statistical aspects of the buckling of imperfection-sensitive structures. J Mech Phys Solids 17(2):111–123
9. Elishakoff I, Arbocz J (1982) Reliability of axially compressed cylindrical shells with random axisymmetric imperfections. Int J Solids Struct 18(7):563–585. https://doi.org/10.1016/0020-7683(82)90040-3
10. Broggi M, Schuëller GI (2011) Efficient modeling of imperfections for buckling analysis of composite cylindrical shells. Eng Struct 33(5):1796–1806. https://doi.org/10.1016/j.engstruct.2011.02.019
11. Schenk CA, Schuëller GI (2003) Buckling analysis of cylindrical shells with random geometric imperfections. Int J Non-Linear Mech 38(7):1119–1132. https://doi.org/10.1016/S0020-7462(02)00057-4
12. Schenk CA, Schuëller GI (2007) Buckling analysis of cylindrical shells with cutouts including random boundary and geometric imperfections. Comput Methods Appl Mech Eng 196(35–36):3424–3434. https://doi.org/10.1016/j.cma.2007.03.014
13. Lauterbach S, Fina M, Wagner W (2018) Influence of stochastic geometric imperfections on the load-carrying behaviour of thin-walled structures using constrained random fields. Comput Mech 62(5):1107–1125. https://doi.org/10.1007/s00466-018-1554-0
14. Fenton GA (1999) Random field modeling of cpt data. J Geotech Geoenviron Eng 125(6):486–498. https://doi.org/10.1061/(ASCE)1090-0241(2000)126:12(1212)
15. Feng C, Valdebenito MA, Chwała M, Liao K, Broggi M, Beer M (2024) Efficient slope reliability analysis under soil spatial variability using maximum entropy distribution with fractional moments. J Rock Mech Geotech Eng 16(4):1140–1152. https://doi.org/10.1016/j.jrmge.2023.09.006
16. Botte W, Vereecken E, Caspeele R (2023) Random field modelling of spatial variability in concrete - a review. Struct Infrastruct Eng, 1–14. https://doi.org/10.1080/15732479.2023.2248102
17. DIN EN 1990:2021 Eurocode-basis of structural and geotechnical design. DIN-Normenausschuss Bauwesen (NABau) (2021)
18. Fina M (2020) Polymorphe Unschärfemodellierung in der nichtlinearen Strukturmechanik - Stabilität von Schalentragwerken, räumliche Variabilität und Metamodellierung. Dissertation, Institut für Baustatik, Karlsruher Institut für Technologie. https://doi.org/10.5445/IR/1000129960
19. Fina M, Weber P, Wagner W (2020) Polymorphic uncertainty modeling for the simulation of geometric imperfections in probabilistic design of cylindrical shells. Struct Saf 82:101894. https://doi.org/10.1016/j.strusafe.2019.101894
20. Fina M, Panther L, Weber P, Wagner W (2021) Shell buckling with polymorphic uncertain surface imperfections and sensitivity analysis. ASCE-ASME J Risk Uncertain Eng Syst Part B: Mech Eng 7(2):020909. https://doi.org/10.1115/1.4050165
21. Fina M, Wagner W, Graf W (2023) On polymorphic uncertainty modeling in shell buckling. Comput-Aided Civ Infrastruct Eng 38:2632–2647. https://doi.org/10.1111/mice.13054
22. Freitag S, Edler P, Kremer K, Meschke G (2020) Multilevel surrogate modeling approach for optimization problems with polymorphic uncertain parameters. Int J Approx Reason 119:81–91. https://doi.org/10.1016/j.ijar.2019.12.015
23. Freitag S, Edler P, Kremer K, Hofmann M, Meschke G (2018) Optimization approaches for durable reinforced concrete structures

considering interval and stochastic parameter uncertainty. PAMM 18(1):e201800444. https://doi.org/10.1002/pamm.201800444
24. Edler P, Freitag S, Kremer K, Meschke G (2019) Optimization approaches for the numerical design of structures under consideration of polymorphic uncertain data. ASCE-ASME J Risk Uncertain Eng Syst Part B: Mech Eng 5(4):041013. https://doi.org/10.1115/1.4044153
25. Schietzold FN, Graf W, Kaliske M (2021) Multi-objective optimization of tree trunk axes in glulam beam design considering fuzzy probability-based random fields. ASCE-ASME J Risk Uncertain Eng Syst, Part B: Mech Eng 7(2):020913. https://doi.org/10.1115/1.4050370
26. Fina M, Lauff C, Wagner W (2022) Optimal shell design with polymorphic uncertain parameters. In: 8th International Symposium on Reliability Engineering and Risk Management. ISRERM. Research Publishing Services, Hannover, pp 345–349. https://doi.org/10.3850/978-981-18-5184-1_MS-12-019-cd
27. Faes MGR, Fina M, Valdebenito MA, Lauff C, Wagner W, Freitag S, Beer M (2022) Bounding failure probabilities in imprecise stochastic FE models. In: Beer, M., Zio, E., Phoon, K.-K., Ayyub, B.M. (eds.) Proceedings of the 8th International Symposium on Reliability Engineering and Risk Management (ISRERM), September 4-7, 2022, Hannover, Germany. Research Publishing. https://doi.org/10.3850/978-981-18-5184-1_MS-15-141-cd
28. Fina M, Lauff C, Faes MGR, Valdebenito MA, Wagner W, Freitag S (2023) Bounding imprecise failure probabilities in structural mechanics based on maximum standard deviation. Struct Saf 101:102293
29. Zhong K, Navarro JG, Govindjee S, Deierlein GG (2023) Surrogate modeling of structural seismic response using probabilistic learning on manifolds. Earthq Eng & Struct Dyn 52(8):2407–2428. https://doi.org/10.1002/eqe.3839
30. Gudipati VK, Cha EJ (2021) Surrogate modeling for structural response prediction of a building class. Struct Saf 89:102041. https://doi.org/10.1016/j.strusafe.2020.102041
31. Schweizer M, Fina M, Wagner W, Kasic S, Freitag S (2024) Uncertain pedestrian load modeling for structural vibration assessment in footbridge design. Eng Struct 311:118070. https://doi.org/10.1016/j.engstruct.2024.118070
32. Fina M, Faes MGR, Valdebenito MA, Wagner W, Broggi M, Beer M, Freitag S (2023) Uncertainty quantification of buckling loads of thin and slender structures applying linear and nonlinear analysis. In: 14th International Conference on Applications of Statistics and Probability in Civil Engineering, July 09-13, 2023, Dublin, Ireland
33. Tahir ZUR, Mandal P, Adil MT, Naz F (2021) Application of artificial neural network to predict buckling load of thin cylindrical shells under axial compression. Eng Struct 248:113221. https://doi.org/10.1016/j.engstruct.2021.113221
34. Nguyen T-A, Ly H-B, Mai H-VT, Tran VQ (2021) Using ANN to estimate the critical buckling load of y shaped cross-section steel columns. Sci Program 2021:1–8. https://doi.org/10.1155/2021/5530702
35. Shahin RI, Ahmed M, Yehia SA, Liang QQ (2023) Ann model for predicting the elastic critical buckling coefficients of prismatic tapered steel web plates under stress gradients. Eng Struct 294:116794. https://doi.org/10.1016/j.engstruct.2023.116794
36. He X, Xu H, Sabetamal H, Sheng D (2020) Machine learning aided stochastic reliability analysis of spatially variable slopes. Comput Geotech 126:103711. https://doi.org/10.1016/j.compgeo.2020.103711
37. He X, Wang F, Li W, Sheng D (2021) Efficient reliability analysis considering uncertainty in random field parameters: trained neural networks as surrogate models. Comput Geotech 136:104212. https://doi.org/10.1016/j.compgeo.2021.104212
38. Hao P, Duan Y, Liu D, Yang H, Liu D, Wang B (2023) Image-driven intelligent prediction of buckling behavior for geometrically imperfect cylindrical shells. AIAA J 61(5):2266–2280. https://doi.org/10.2514/1.J062470
39. Sudret B, Der Kiureghian A (2000) Stochastic finite element methods and reliability - a state-of-the-art report. University of California, Berkeley, Department of Civil and Environmental Engineering
40. Vanmarcke E (2010) Random fields: analysis and synthesis. World Scientific, Singapore
41. Zhang J, Ellingwood B (1994) Orthogonal series expansions of random fields in reliability analysis. J Eng Mech 120(12):2660–2677. https://doi.org/10.1061/(ASCE)0733-9399(1994)120:12(2660)
42. Böhm M (2024) Buckling analysis of suction buckets: influence of uncertainty in imperfections and soil parameters. Dissertation, Fakultät für Bauingenieurwesen und Geodäsie, Gottfried Wilhelm Leibniz Universität Hannover. https://doi.org/10.15488/17658
43. Maes MA, Breitung K, Dann MR (2021) At issue: the Gaussian autocorrelation function. In: Matos, J.C., et al. 18th International Probabilistic Workshop. IPW 2021. Lecture Notes in Civil Engineering, vol 153, Springer
44. Faes MGR, Broggi M, Spanos PD, Beer M (2022) Elucidating appealing features of differentiable auto-correlation functions: a study on the modified exponential kernel. Probab Eng Mech 69:103269. https://doi.org/10.1016/j.probengmech.2022.103269
45. Baitsch M (2003) Optimierung druckbeanspruchter stabtragwerke unter berücksichtigung geometrischer imperfektionen. Dissertation, Ruhr-Universität Bochum
46. Wagner W (1995) A note on FEM buckling analysis. Commun Numer Methods Eng 11(2):149–158
47. Riks E (1972) The application of Newton's method to the problem of elastic stability. J Appl Mech 39(4):1060–1065. https://doi.org/10.1115/1.3422829
48. Wagner W (1991) A path-following algorithm with quadratic predictor. Comput Struct 39(3–4):339–348
49. Taylor RL (2024) FEAP. http://www.ce.berkeley.edu/projects/feap/
50. Adeli H (2001) Neural networks in civil engineering: 1989–2000. Comput-Aided Civ Infrastruct Eng 16(2):126–142. https://doi.org/10.1111/0885-9507.00219
51. Basheer IA, Hajmeer M (2000) Artificial neural networks: fundamentals, computing, design, and application. J Microbiol Methods 43(1):3–31. https://doi.org/10.1016/S0167-7012(00)00201-3
52. The MathWorks Inc.: MATLAB Version: 24.2.0 (R2024a). https://www.mathworks.com
53. Levenberg K (1944) A method for the solution of certain non-linear problems in least squares. Q Appl Math 2(2):164–168. https://doi.org/10.1090/qam/10666
54. Marquardt DW (1963) An algorithm for least-squares estimation of nonlinear parameters. J Soc Ind Appl Math 11(2):431–441. https://doi.org/10.1137/0111030
55. Timoshenko SP, Geere JM (1961) Theory of elastic stability. McGraw Hill